09:43:11 OCA PAD AMENDMENT - PROJECT HEADER INFORMATION 03/26/97

Active

Project #: E-25-W01 Cost share #: E-25-365 Rev #: 8
Center # : 10/24-6-R7903-0A0 Center shr #: 10/22-1-F7903-0A0 OCA file #:
Work type : RES
Contract#: F49620-93-1-0495 Mod #: P00002 Document : GRANT
Prime #: Contract entity: GTRC

Subprojects ? : Y CFDA: 12.800
Main project #: PE #:

Project unit: MECH ENGR Unit code: 02.010.126
Project director(s):
GLEZER A MECH ENGR (404)894-3262

Sponsor/division names: AIR FORCE / BOLLING AFB, DC
Sponsor/division codes: 104 / 001

Award period: 930815 to 970214 (performance) 970414 (reports)

Sponsor amount	New this change	Total to date
Contract value	0.00	121,716.00
Funded	0.00	121,716.00
Cost sharing amount		32,603.00

Does subcontracting plan apply ?: N

Title: MEMS-BASED DIAGNOSTICS FOR TORBULENT SHEAR FLOWS

PROJECT ADMINISTRATION DATA

OCA contact: Anita D. Rowland 894-4820

Sponsor technical contact

DR JAMES M. MCMICHAEL
(202)767-4936

AFOSR/NA
110 DUNCAN AVENUE
SUITE B115
BOLLING AFB, DC 20332-0001

Sponsor issuing office

JENNIFER BELL
(202)767-6836

AFOSR/PKA
110 DUNCAN AVENUE
SUITE B115
BOLLING AFB, DC 20332-0001
FAX: 202.404.7951

Security class (U,C,S,TS) : U ONR resident rep. is ACO (Y/N): N
Defense priority rating : N/A N/A supplemental sheet
Equipment title vests with: Sponsor GIT X
TITLE <$5,000 WITH GIT AT ACQUISITION.
Administrative comments -
MOD P-2 WARDS A NCE THRU 2.14.97

Closeout Notice Date 20-MAY-1997

Project Number E-25-W01 Doch Id 32443

Center Number 10/24-6-R7903-0A0

Project Director GLEZER, ARI

Project Unit MECH ENGR

Sponsor AIR FORCE/BOLLING AFB, DC

Division Id 3346

Contract Number F49620-93-1-0495 Contract Entity GTRC

Prime Contract Number

Title MEMS-BASED DIAGNOSTICS FOR TORBULENT SHEAR FLOWS

Effective Completion Date 14-FEB-1997 (Performance) 14-APR-1997 (Reports)

Closeout Action:	Y/N	Date Submitted
Final Invoice or Copy of Final Invoice	Y	
Final Report of Inventions and/or Subcontracts	Y	
Government Property Inventory and Related Certificate	Y	
Classified Material Certificate	N	
Release and Assignment	N	
Other	N	

Comments

Distribution Required:

Project Director/Principal Investigator	Y
Research Administrative Network	Y
Accounting	Y
Research Security Department	N
Reports Coordinator	Y
Research Property Team	Y
Supply Services Department	Y
Georgia Tech Research Corporation	Y
Project File	Y

NOTE: Final Patent Questionnaire sent to PDPI

E-25-W01 2/a

Georgia Tech

Office of Grants and Contracts Accounting

Georgia Institute of Technology
190 Bobby Dodd Way
Atlanta, Georgia 30332-0259
USA
404•894•4624; 2629
Fax: 404•894•5519

January 4, 1996

Air Force Office of Scientific Research
AFOSR / PKA
110 Duncan Avenue, Suite B115
Attn: Jennifer Bell
Bolling AFB, D. C. 20332-0001

Subject: Grant No. F49620-93-1-0495

Dear Ms. Bell:

Enclosed are interim Financial Status Reports (SF 269) for the above noted grant for the periods ending 8/14/94 and 8/14/95.

If you have any questions or require additional information, please contact Kate Edwards at (404) 894-5522.

Sincerely,

David V. Welch, Director
Grants and Contracts Accounting

DVW/ke

Enclosures

File: E-25-W01/246R79030A0
OCA - Anita Rowland- Mailcode 0420
OCA - Wanda Simon - Mailcode 0420

FINANCIAL STATUS REPORT

(SHORT FORM)

(Follow instructions on the back)

1. FEDERAL AGENCY AND ORGANIZATIONAL ELEMENT TO WHICH REPORT IS SUBMITTED	2. FEDERAL GRANT OR OTHER IDENTIFYING NUMBER ASSIGNED BY FEDERAL AGENCY	OMB Approval No.	PAGE	OF
U S AIR FORCE	F49620-93-1-0495	0348-0039	1	1 Pages

3. RECIPIENT ORGANIZATION (Name and complete address, including ZIP code)
GEORGIA TECH RESEARCH CORPORATION, P.O. BOX 100117, ATLANTA, GA 30384

4. EMPLOYER IDENTIFICATION NUMBER	5. RECIPIENT ACCOUNT NUMBER OR IDENTIFYING NUMBER	6. FINAL REPORT	7. BASIS
58-0603146	E-25-W01/246R79030A0	[ ] YES [X] NO	[X] CASH [ ] ACCRUAL

8. PROJECT/GRANT PERIOD (See instructions)		9. PERIOD COVERED BY THIS REPORT	
FROM: (Month, Day, Year)	TO: (Month, Day, Year)	FROM: (Month, Day, Year)	TO: (Month, Day, Year)
8/15/93	8/14/96	8/15/93	8/14/94

10. TRANSACTIONS:	I PREVIOUSLY REPORTED	II THIS PERIOD	III CUMULATIVE
a. Total Outlays	0.00	3,517.64	3,517.64
b. Recipient share of outlays	0.00	0.00	0.00
c. Federal share of outlays	0.00	3,517.64	3,517.64
d. Total unliquidated obligations			0.00
e. Recipient share of unliquidated obligations			0.00
f. Federal share of unliquidated obligations			1,165.39
g. Total Federal share (sum of lines c and f)			4,683.03
h. Total Federal funds authorized for this funding period			121,716.00
i. Unobligated balance of federal funds (Line h minus line g)			117,032.97

11. Indirect Expense	a. Type of Rate (Place "X" in appropriate box)							
	[ ] Provisional		[ ] Predetermined		[ ] Final		[X] Fixed	
	b. Rate		c. Base	d. Total Amount		e. Federal Share		
	FY 1995	40.00%	2,512.60	1,005.04		1,005.04		

12. Remarks: Attach any explanations deemed necessary or information required by Federal sponsoring agency in compliance with governing legislation.

13. Certification: I certify to the best of my knowledge and belief that this report is correct and complete and that all outlays and unliquidated obligations are for the purposes set forth in the award documents.

Typed or Printed Name and Title	Telephone (Area code, number and extension)
David V. Welch, Director Grants and Contracts Accounting	(404) 894-2629
Signature of Authorized Certifying Official	Date Report Submitted REISSUED 1/4/96 original dated 1/17/95

NSN 7540-01-218-4387 269-201 Standard Form 269A (rev 4-88)

Prescribed by OMB Circulars A-102 and A-110

Questions concerning this report should be directed to Kate Edwards (404) 894-5522.

E-25-W01 3

REPORT OF INVENTIONS AND SUBCONTRACTS

(Pursuant to "Patent Rights" Contract Clause) (See Instructions on Reverse Side.)

Form Approved
OMB No. 0704-0297
Expires Jun 30, 1992

1a. NAME OF CONTRACTOR / SUBCONTRACTOR	c. CONTRACT NUMBER	2a. NAME OF GOVERNMENT PRIME CONTRACTOR	c. CONTRACT NUMBER	3. TYPE OF REPORT (X one)
Georgia Tech Research Corp.	F49620-93-1-0495			X a. INTERIM ☐ b. FINAL
b. ADDRESS (Include ZIP Code)	**d. AWARD DATE (YYMMDD)**	**b. ADDRESS (Include ZIP Code)**	**d. AWARD DATE (YYMMDD)**	**4. REPORTING PERIOD (YYMMDD)**
Atlanta, GA 30332	930815			a. FROM 930815
				b. TO 940814

SECTION I – SUBJECT INVENTIONS

5. "SUBJECT INVENTIONS" REQUIRED TO BE REPORTED BY CONTRACTOR / SUBCONTRACTOR (If "None," so state)

a. NAME(S) OF INVENTOR(S) (Last, First, MI)	b. TITLE OF INVENTION(S)	c. DISCLOSURE NO., PATENT APPLICATION SERIAL NO. OR PATENT NO.	d. ELECTION TO FILE PATENT APPLICATIONS				e. CONFIRMATORY INSTRUMENT OR ASSIGNMENT FORWARDED TO CONTRACTING OFFICER	
			(1) United States		(2) Foreign			
			(a) Yes	(b) No	(a) Yes	(b) No	(1) Yes	(2) No
	None							

f. EMPLOYER OF INVENTOR(S) NOT EMPLOYED BY CONTRACTOR / SUBCONTRACTOR		g. ELECTED FOREIGN COUNTRIES IN WHICH A PATENT APPLICATION WILL BE FILED	
(1) (a) Name of Inventor (Last, First, MI)	(2) (a) Name of Inventor (Last, First, MI)	(1) Title of Invention	(2) Foreign Countries of Patent Application
(b) Name of Employer	(b) Name of Employer		
(c) Address of Employer (Include ZIP Code)	(c) Address of Employer (Include ZIP Code)		

SECTION II – SUBCONTRACTS (Containing a "Patent Rights" clause)

6. SUBCONTRACTS AWARDED BY CONTRACTOR / SUBCONTRACTOR (If "None," so state)

a. NAME OF SUBCONTRACTOR(S)	b. ADDRESS (Include ZIP Code)	c. SUBCONTRACT NO.(S)	d. DFAR "PATENT RIGHTS"		e. DESCRIPTION OF WORK TO BE PERFORMED UNDER SUBCONTRACT(S)	f. SUBCONTRACT DATES (YYMMDD)	
			(1) Clause Number	(2) Date (YYMM)		(1) Award	(2) Estimated Completion
	None						

SECTION III – CERTIFICATION

7. CERTIFICATION OF REPORT BY CONTRACTOR / SUBCONTRACTOR (Not required if ☐ Small Business or X Non-Profit organization.) (X appropriate box)

a. NAME OF AUTHORIZED CONTRACTOR / SUBCONTRACTOR OFFICIAL (Last, First, MI)	c. I certify that the reporting party has procedures for prompt identification and timely disclosure of "Subject inventions," that such procedures have been followed and that all "Subject Inventions" have been reported.	
Rowland, Anita D.		
b. TITLE	**d. SIGNATURE**	**e. DATE SIGNED**
Contracting Officer		941129

DD Form 882, OCT 88

DD FORM 882 INSTRUCTIONS

GENERAL

This form is for use in submitting INTERIM and FINAL invention reports to the Contracting Officer and for use in the prompt notification of the award of subcontracts containing a "Patent Rights" clause. If the form does not afford sufficient space, multiple forms may be used or plain sheets of paper with proper identification of information by Item Number may be attached.

An INTERIM report is due at least every 12 months from the date of contract award and shall include (a) a listing of "Subject Inventions" during the reporting period, (b) a certification of compliance with required invention identification and disclosure procedures together with a certification of reporting of all "Subject Inventions," and (c) any required information not previously reported on subcontracts awarded during the reporting period and containing a "Patent Rights" clause.

A FINAL report is due within 6 months if contractor is a small business firm or domestic nonprofit organization and within 3 months for all others after completion of the contract work and shall include (a) a listing of all "Subject Inventions" required by the contract to be reported, and (b) any required information not previously reported on subcontracts awarded during the course of or under the contract and containing a "Patent Rights" clause.

While the form may be used for simultaneously reporting inventions and subcontracts, it may also be used for reporting, promptly after award, subcontracts containing a "Patent Rights" clause.

Dates shall be entered where indicated in certain Items on this form and shall be entered in four or six digit numbers in the order of year and month (YYMM) or year, month and day (YYMMDD). Example: April 1986 should be entered as 8604 and April 15, 1986 should be entered as 860415.

Item 1a. Self-explanatory.

Item 1b. Self-explanatory.

Item 1c. If "same" as item 2c, so state.

Item 1d. Self-explanatory.

Item 2a. If "same" as item 1a, so state.

Item 2b. Self-explanatory.

Item 2c. Procurement Instrument Identification (PII) number of contract (DFAR 4.7003).

Item 2d thru 5e. Self-explanatory.

Item 5f. The name and address of the employer of each inventor not employed by the contractor or subcontractor is needed because the Government's rights in a reported invention may not be determined solely by the terms of the "Patent Rights" clause in the contract.

Example 1: If an invention is made by a Government employee assigned to work with a contractor, the Government rights in such an invention will be determined under Executive Order 10096.

Example 2: If an invention is made under a contract by joint inventors and one of the inventors is a Government employee, the Government's rights in such an inventor's interest in the invention will also be determined under Executive Order 10096, except where the contractor is a small business or nonprofit organization, in which case the provisions of Section 202 (e) of P.L. 96-517 will apply.

Item 5g (1). Self-explanatory.

Item 5g (2). Self-explanatory with the exception that the contractor or subcontractor shall indicate, if known at the time of this report, whether applications will be filed under either the Patent Cooperation Treaty (PCT) or the European Patent Convention (EPC). If such is known, the letters PCT or EPC shall be entered after each listed country.

Item 6a. Self-explanatory.

Item 6b. Self-explanatory.

Item 6c. Self-explanatory.

Item 6d. Patents Rights Clauses are located in FAR 52.227.

Item 6e thru 7b. Self-explanatory.

Item 7c. Certification not required by small business firms and domestic nonprofit organizations.

E-25-W01
1, 2

REPORT DOCUMENTATION PAGE

Form Approved
OMB No. 0704-0188

1. AGENCY USE ONLY (Leave Blank)	2. REPORT DATE	3. REPORT TYPE AND DATES COVERED
		Progress Report

4. TITLE AND SUBTITLE

MEMS Based Diagnostics for Turbulent Shear Flows

5. FUNDING NUMBERS

PE-61102F
PR-2307
SA-BS G-AFOSR
F49620-93-1-0495

6. AUTHOR(S)

A. Glezer, M.G. Allen and M.A. Brooke

7. PERFORMING ORGANIZATION NAME(S) AND ADDRESS(ES)

Georgia Tech Research Corporation
Atlanta, GA 30332

8. PERFORMING ORGANIZATION REPORT NUMBER

9. SPONSORING/MONITORING AGENCY NAME(S) AND ADDRESS(ES)

Dr. J.M. McMichael
AFOSR
Building 410
Bolling AFB, DC 20332-6440

10. SPONSORING/MONITORING AGENCY REPORT NUMBER

11. SUPPLEMENTARY NOTES

12a. DISTRIBUTION/AVAILABILITY STATEMENT

Unclassified; Distribution Unlimited

12b. DISTRIBUTION CODE

13. ABSTRACT (Maximum 200 words)

This report deals with progress made in two areas in MEMS-based diagnostics for turbulent shear flows. In the first section of the report, the progress made on neural net processing and design is outlined. A pipelined processor for real time charge-coupled display image processing is described. The device has been designed and laid out for fabrication by a standard silicon chip foundry (MOSIS). In the second section of the report, the progress made in fabrication of MEMS devices for flow control is discussed. Successful fabrication and initial characterization of the MEMS-based micromachined jets (microjets) has been accomplished. The microjets consist of an orifice 150-300 microns in diameter situated atop an actuator cavity which is bounded by a flexible membrane. Vibration of the membrane using either electrostatic or piezoelectric drive results in a nominally round turbulent air jet formed normal to the microjet orifice. Microjets with velocities of 17 m/s and coherent to lengths exceeding 500 diameters were achieved. The Reynolds number at a distance of 15 diameters is estimated at approximately 1400.

14. SUBJECT TERMS

MEMS, micromachining, neural network, CCD, jets, flow

15. NUMBER OF PAGES

16. PRICE CODE

17. SECURITY CLASSIFICATION OF REPORT	18. SECURITY CLASSIFICATION OF THIS PAGE	19. SECURITY CLASSIFICATION OF ABSTRACT	20. LIMITATION OF ABSTRACT
unclassified	unclassified	unclassified	UL

AUGMENTATION AWARDS FOR SCIENCE & ENGINEERING RESEARCH TRAINING (ASSERT) REPORTING FORM

The Department of Defense (DoD) requires certain information to evaluate the effectiveness of the AASERT Program. By accepting this Grant which bestows the ASSERT funds, the Grantee agrees to provide 1) a brief (not to exceed one page) narrative technical report of the research training activities of the AASERT-funded student(s) and 2) the information should be provided to the Government's technical point of contract by each annual anniversary of the AASERT award date.

1. Grantee identification data: (R&T and Grant numbers found on Page 1 of Grant)

1. Grantee identification data: (R&T and Grant numbers found on Page 1 of Grant)

a. Georgia Institute of Technology
University Name

b. F49620-93-1-0495
Grant Number

c. _____
R&T Number

d. Ari Glezer
P.I. Name

e. From: 15 Aug 93 To: 14 Aug 94
AASERT Reporting Period

NOTE: Grant to which AASERT award is attached is referrred to hereafter as "Parent Agreement".

2. Total funding of the Parent Agreement and the number of full-time equivalent graduate students (FTEGS) supported bt the Parent Agreement during the 12-month period prior to the AASERT award date.

a. Funding: $ 160,000

b. Number FTEGS: 2

3. Total funding of the Parent Agreement and the number of FTEGS supported by the Parent Agreement during the current 12-month period.

a. Funding: $ 101,067

b. Number FTEGS: 2

4. Total AASERT funding and the number of FTEGS and undergraduate students (UGS) supported by AASERT funds during the current 12-month reporting period.

a. Funding: $ 39,848

b. Number FTEGS: 2

c. Number UGS: _____

VERIFICATION STATEMENT: I hereby verify that all students supported by the AASERT award are U.S. Citizens.

_____ Dec 1, 1994
Principal Investigator Date

ASSERT Student Progress

There are two students currently being supported on the AASERT grant. Mr. Brent Buchanan is under the direction of Prof. Martin Brooke, and Mr. David Coe is under the direction of Prof. Mark Allen. Each of the students is evaluated below.

Student Name:Brent Buchanan
Citizenship: US
Grades: 3.9/4.0

Abstract of Student's Work:

A prototype hybrid analog digital pipelined convolution processor has been designed and is being fabricated. This type of pipelined processor can take advantage of the serial nature of the CCD image output to perform real time processing of CCD images. The 2.2 x 2.3 millimeter IC will perform real-time 5x5 convolutions on CCD images of dimension 32xN where N is an arbitrary dimension.

Student Name: David Coe
Citizenship: US
Grades: 3.7/4.0

Abstract of Student's Work:

David Coe's work to date involves the successful fabrication and initial characterization of the micromachined jets (microjets) described in this report. The microjets were fabricated using standard silicon micromachining techniques and consist of an orifice situated atop an actuator cavity which is bounded by a flexible membrane. Typical microjet orifice sizes range from 150-300 microns. Vibration of the membrane using either electrostatic or piezoelectric drive results in a nominally round turbulent air jet formed normal to the microjet orifice. Initial characterization was performed using a miniature total pressure tube and a conventional miniature hot wire sensor. Microjets with velocities of 17 m/s and coherent to lengths exceeding 500 diameters were achieved. The microjet Reynolds number at a distance of 15 diameters is estimated at approximately 1400.

Evaluation of Student's Work:

David Coe has performed the above work extremely well. Since the beginning of the grant, he has not only developed the technology described above, but he has presented it to two different communities, the MEMS community and the fluid mechanics community, at two important conferences. We have every expectation that David will continue to perform superlatively, and be able to complete microjet work for his Ph.D. thesis work.

I. Technical Report Structure

The technical section of this report is divided into several sections. In Section II, the progress made on neural net processing and design is outlined. In Section III, the progress made in fabrication of MEMS devices for flow control is discussed. In Section IV, plans for future work over the next year are discussed. All figures referred to in the text are collected at the end of the report.

II. Pipelined processor for real time CCD Image processing

Pipelined processors can take advantage of the serial nature of the CCD image output to perform real time processing of CCD images. The pipelining approach takes data at the rate at which the CCD imager generates it, stores sufficient data to enable the necessary computations, processes the data, and the generates the processed images at the same rate at which they produced by the CCD imager. The only delay is the initial delay time taken to accumulate sufficient data for processing to begin, after that the images are produced in real time.

Most image processing functions can be implemented with a few basic types of image operations: differencing, accumulating, resizing, and convolutions. Each of these operations has a different pipelined processor representation. In Figure II.1 a pipelined processor for image convolutions is presented. This processor performs 8x8 convolutions on large images at the full frame rate. For an 8x8 convolution an 8xN segment of an NxM image must be stored on the processor before processing can begin. This is stored in the digital shift registers shown in Figure II.1.

To maintain real time operation the convolution processor must perform 64 multiplies and one accumulate in the time the CCD images outputs one pixels worth of image data. We have chosen a hybrid analog digital approach to performing these computations. This gives us a low power, small size implementation.

A prototype hybrid analog digital pipelined convolution processor has been designed and is being fabricated. The block diagram of one row of the processor appears in Figure II.2. This row corresponds to one horizontal row of the processing in Figure II.1. The 2.2 x 2.3 millimeter IC layout for the IC appears in Figure II.3. This prototype IC performs 5x5 convolutions on images 32xN where N is an arbitrary dimension.

The heart of this device is the shift register. Its purpose is to both maintain the integrity of the data and to automatically preserve the correct spatial relationships between the pixels of the image as they are shifted over the convolution window. As a digital shift register, the data is identically replicated as it shifts through the device, a feature that scales to any length digital shift register.

The spatial relationship of the data is maintained by assuming a fixed and known input image size and then positioning the convolution components along the shift register accordingly. This particular device is intended for a 32 pixel wide image, so output taps to feed the convolution multipliers begin at intervals spaced every 32 positions along the shift register. This row-wise linearization of the image (assuming that the data is row-wise shifted into the device) then forces each image pixel to traverse the entire shift register length, and the 32 pixel spacing thus corresponds to the same column location in the preceding row of the 32 pixel wide image. As the shift register is clocked, the window of the convolution kernel effectively sweeps over the entire image, performing a circular type convolution as the kernel window bridges the opposite sides of the image, with the modification to the standard circular convolution that the rows are spiral connected such that the kernel window is forced down one row with each revolution of the circle. The output during the edge bridging portion of the convolution can optionally be ignored without the loss of data in the output stream since the convolution of an NxN image with a MxM convolution kernel naturally produces an (N-M)x(N-M) output, where M is also the distance covered by the kernel when the edges are bridged.

Among the considerations in designing the shift register were timing, reliability, and layout size. To avoid clock timing problems and the consequential reliability issues, a two-phase clock was chosen as the first architectural element. Inverters were chosen for signal reconstruction (gain) since they are physically small devices and easily allow for the incorporation of a transfer gate on their output at little extra cost in physical size. The implications of signal inversion are not a problem since a minimum of two storage stages are necessary in two-phase systems to achieve avoidance of signal feed through, and with the use of an inverter in both half-stages, the original signal polarity is restored within each register in the chain. Each shift register stage then consists of two identical sub-units, each of which contains an inverter and transfer gate. The data is dynamically stored on the parasitic input capacitance to the inverter stages and is isolated by turning off the transfer gate at the output of the previous inverter. The nature of the two-phase clock prevents no more than one of the pair of transmission gates in each register from being active at a time, allowing the data to orderly ripple through the shift register chain at the rate of one half of a

register per clock phase. The effective size of the one bit shift register's standard cell in this device is 28 μm by 52 μm.

Two considerations led to the choice of the 5 bit word size (shift register width) for this device; both relate to physical device size restrictions. The best accuracy per unit area D/A converter that we have tested to date is a five bit converter roughly 40 lambda by 150 lambda. The use of this converter coupled with the 2 mm by 2 mm usable area of a MOSIS Tiny-Chip (lambda = 1.0) dictated that little more than 160 5-bit pixel shift registers (160=5x32), allowing for between a 5x5 to a 5x7 convolution kernel, could be incorporated into this revision device. Each of the five 32-pixel long sections of the shift register is identical, with the exception that the last section is only 16 pixels wide, since no data taps for the convolution components are required beyond that point. The output of each of the other 32-pixel long sections in turn feed into the input of the next section, naturally.

Each clock phase is buffered and inverted in parallel, one buffer per phase per 32-pixel section, prior to distribution to each of the five 32-pixel sections of the shift register. To minimize skew between the each of the phases and its inverse, the non-inverted clock signal is fed through a transmission gate of equal size to the inverter.

Two sets of taps exist for passing data from the shift register to the convolution components. One set feeds to memory cells which store the data from the tapped locations in the shift register when the load signal is activated. The memory cells consist of two inverters that are either configured into a series loop that is isolated from signals from the shift register when the load signal is not active (storage mode), or an open loop that is driven by the signals from the shift register when the load signal is active (read mode). The data in the memory cells performs as the stored weight values of the convolution kernel, and it is not inverted in the storage process prior to being transferred to the weight D/A converters.

The weight D/A converters are the previously mentioned 40 μm x 150 μm five bit converters that provide a 32-level current output. The D/As are the current division type, with the bias current independently mirrored to each of the 25 weight D/A converters (i.e., a bias current is distributed across the device instead of a bias voltage). The 32 level output current is in turn used as the bias current to an identical 5-bit D/A converter that's digital input is driven directly by five adjacent taps (one per convolution weight, each tap is 5 bits wide) at the head of each 32-pixel section shift register. The paired D/A converters thus form an MDAC, with the weight D/A being driven by an adjustable bias current and statically stored digital value, and the operand D/A being driven by the current output of the

weight D/A and a dynamically stored digital value from the corresponding location in the shift register.

The current outputs from each row of the convolution window are tied together and then independently fed of chip, one output per row. Additionally, as a check on the integrity and operation of the digital shift register, four of the bits output from the last register are buffered and also fed off chip.

III. Progress Made on MEMS Structures

The progress made on MEMS structures is detailed a recently published paper by D.J. Coe, M.J. Trautman, M.G. Allen, and A. Glezer, entitled 'Micromachined Jets for Manipulation of Macro Flows'. This paper was presented at the 1996 Solid State Sensors and Actuators Workshop, Hilton Head, South Carolina. We have also submitted a proposal to AFOSR involving the use of micromachined jets for application to the aero-optics problem, and a proposal to ARPA involving the use of micromachined jets for application in three areas: fanless microelectronic cooling; micromixing (including the aero-optics problem); and modification of aerodynamic surfaces with no moving parts.

The MEMS work to date involves the successful fabrication and initial characterization of micromachined jets (microjets) fabricated for use in macro flow control and other applications. The microjets were fabricated using standard silicon micromachining techniques and consist of an orifice situated atop an actuator cavity which is bounded by a flexible membrane. Typical microjet orifice sizes range from 150-300 microns. Vibration of the membrane using either electrostatic or piezoelectric drive results in a nominally round turbulent air jet formed normal to the microjet orifice. An important feature of the jet is that it is formed without net mass injection by an oscillatory flow that is acoustically induced near the edge of the orifice. Initial characterization was performed using a miniature total pressure tube and a conventional miniature hot wire sensor. Microjets with velocities of 17 m/s and coherent to lengths exceeding 500 diameters were achieved. The microjet Reynolds number at a distance of 15 diameters is estimated at approximately 1400.

Introduction

While there is no question that one of the most important application areas for microactuators is the control of macro-events, these actuators usually generate insufficient force to directly realize control authority. Thus, some type of mechanical amplification is

required. An attractive means for the amplification of the actuator output is its coupling to inherently unstable pressure or flow systems. If system operating points are carefully chosen, the relatively small forces generated by a microactuator can be used to create large disturbances in either static, pressure-balanced systems or in free- and wall-bounded shear flows. These concepts have been exploited for years in a number of static and dynamic macro systems such as pressure regulators and fluidic actuators, respectively. More recently Huff et al. [1] have demonstrated the adaptation of a pressure-balanced system to an electrostatically-actuated microvalve.

An example of flow control that illustrates a scaling hierarchy which can be adopted for microactuators is in the area of jet thrust vectoring. Recent experiments by Green and Glezer [2] have demonstrated the utility of millimeter-scale surface actuation for thrust vectoring of larger jets having characteristic length scales that are at least two orders of magnitude larger. Vectoring is accomplished by exploiting hydrodynamic instabilities of the macro-jets near the flow boundary such that the energy necessary for their manipulation is extracted from the mean flow and thus the power input to the actuators is of the order of several milliwatts [3-4]. The efficacy of this technique has been demonstrated in an air jet emanating from a rectangular orifice (7.62 x 1.27 cm) as shown in contour plots of the measured streamwise velocity component in the cross-stream plane (Figure III.1a-III.1c). The unforced jet is shown in Figure III.1a for reference. In Figure III.1b, the jet is forced by and vectored away from the bottom actuators. Time-periodic vectoring is achieved when the input waveforms to the top and bottom actuators are modulated out of phase (Figure III.1c). Recent jet vectoring experiments at Georgia Tech (Smith and Glezer, unpublished) in which the mechanical actuators were replaced with millimeter-scale zero mass flux surface jets have suggested the concept of cascaded control. Namely, that micromachined jet actuators (microjets) be used to manipulate millimeter-scale jets which, in turn, will control larger jets. Arrays of micromachined jets are particularly attractive for such applications because they can be individually addressed and phased. In this paper, we describe some design and fabrication concepts of micromachined jet actuators and include some preliminary measurements of their performance.

Jet Operation

In the present investigation a nominally round turbulent air jet is formed normal to an orifice in a flat plate. An important feature of the jet is that it is formed without net mass injection by an oscillatory flow that is acoustically induced near the edge of the orifice. As in larger-scale geometries (e.g., Ingard and Labate [5]) the jet is synthesized by a train of

vortex rings. Each vortex is formed during the half cycle of the acoustic wavetrain when the orifice velocity is in the streamwise direction and is advected away from the plate under its self-induced velocity. The vortices are formed at the excitation frequency and the jet is synthesized by their interaction downstream from the orifice. In the present work, the acoustic excitation is provided by a diaphragm that is mounted at the bottom of a sealed shallow cylindrical cavity under the orifice plate as described below.

Fabrication

A cross-section of the prototype microjet in shown in Figure III.2. In this design, the orifice and actuator are incorporated into the same wafer. Both electrostatic and piezoelectric drive can be used in this configuration. Although only a single jet is shown in this configuration, extension of this concept to addressable arrays of microjets is straightforward and has been realized by us.

The microjet orifice and actuator hole were anisotropically etched in the wafer as pictured in Figure III.3. Starting with a high resistivity two inch <100> silicon wafer that was polished on both sides, a layer of silicon dioxide 1 micron in thickness was formed using wet thermal oxidation. On the front side a 3000 Å layer of aluminum was deposited using DC sputtering. Photolithography was then used to pattern a square orifice hole in the aluminum. This hole was designed to be 265 microns on a side. Using the patterned aluminum as a mask for infrared alignment, a matching orifice hole was created on the back side of the wafer using photolithography. Using the patterned silicon dioxide as an etch mask, the jet orifice was anisotropically etched using a 20% potassium hydroxide solution in water at 60 °C (Figure III.3b).

Photolithography was then used to pattern a square actuator hole in the back-side oxide 3 mm on a side (Figure III.3c). This hole was anisotropically etched to a depth of 15 microns using a timed etch consisting of 20% potassium hydroxide in water at 50 °C (Figure III.3d). The wafer was then re-oxidized using thermal oxidation such that a layer of 2500 Å of silicon dioxide was formed in the etched region. A layer of aluminum 3000 Å in thickness was then sputtered on the back side of the wafer to act as an electrode for electrostatic actuation. A layer of polyimide film was bonded to the back side of the wafer to form the flexible actuation diaphragm. This polyimide film was then coated with a layer of 3000 Å of aluminum using DC sputtering to provide the second electrode for electrostatic actuation (Figure III.3e).

For electrostatic actuation, application of voltage between the diaphragm electrode and the electrode on the back side of the wafer was used to realize diaphragm actuation.

Alternatively, a ground plane below the wafer could also be used for actuation; in this case, voltage is applied between the diaphragm electrode and the ground plane. For piezoelectric actuation, the back side of the wafer was fitted with non-vented standoffs and bonded to a commercial piezoelectric transducer. Vibration of the piezoelectric transducer caused pressure fluctuations in the transducer-actuator wafer cavity, thus realizing diaphragm actuation. Both electrostatic and piezoelectric actuation were successful in the creation of microjets. In the case of piezoelectric actuation, the jet output could be modified by the electrostatically actuatable diaphragm. In the jet measurements described below, piezoelectric actuation is used.

Initial Measurement of the Jet Flow

In all experiments reported here, the piezoelectric driver is operated at its nominal 1.3 kHz resonance frequency in its first axisymmetric mode of vibration using a laboratory function generator and a high voltage (max. 120 Vrms) broad band DC amplifier (the present measurements were taken at an excitation level of 42 Vrms). Figure III.4 is a smoke visualization photograph of the jet where the smoke is injected radially near the orifice edge. The field of view measures 89 mm in the streamwise (x) direction and thus corresponds to nearly 500 jet diameters. The jet appears to become turbulent at or near the orifice, and spreads almost linearly with streamwise distance. Large coherent vortical structures are apparent in the far field of the jet. The Reynolds number of the jet based on the centerline velocity and its width at x/D = 15 (see velocity profiles in Figure III.5) is approximately 1400.

The streamwise velocity component was measured using a miniature total pressure tube having inner and outer diameters of 212 μm and 340 μm, respectively. Radial profiles of the time-averaged streamwise velocity were measured at x/D = 15, 25, and 35 using a three-axis traversing mechanism and are shown in Figure III.5. Despite the obvious limitations in spatial resolution and sensor interference, these profiles suggest that the jet is reasonably symmetric about its centerline, and furthermore, when these profiles are plotted in the usual similarity coordinates (Figure III.5b), they appear to collapse reasonably well on top of each other, suggesting that the jet is self-similar. The self-similarity of the flow is further supported by the linear decay of the centerline velocity with streamwise distance for x/D > 15 as shown in Figure III.6 (a line with a slope of -1 is shown for reference). Measurements at x/D < 15 are included for reference as an indication of the spatial limitations of the sensor.

Finally, a spectrum of the centerline (streamwise) velocity was measured at x/D = 40 using a conventional miniature hot wire sensor and is shown in Figure III.7. The spectral component at the excitation frequency and its higher harmonics shows that an oscillatory component of the fluid velocity is prominent even in the far field of the jet. It is noteworthy that the spectrum is virtually featureless below 1000 Hz and that no subharmonics of the excitation frequency are present.

Conclusions

Micromachined jets and jet arrays have been realized using silicon micromachining techniques. These jets can be driven piezoelectrically or electrostatically and can produce velocities on the order of 17 m/s within 15 orifice diameters, and remain established up to 500 diameters or more. Each jet is produced with no mass injection at the edge of an orifice by a vibrating diaphragm and is synthesized by the interaction of a train of vortex rings. Although these jets are formed by the strong oscillatory motions, they appear to become self similar within fifteen orifice diameter from the actuator surface. These microjets show great promise as vehicles by which macro-scale effects can be influenced by microactuators.

References

[1] Huff, M.A., Mettner, M.S., Lober, T.A. and Schmidt, M.A., "A pressure-balanced electrostatically-actuated microvalve," Proceedings of Solid State Sensors and Actuators Conference, Hilton Head, SC, June, 1990.

[2] Green, S. M., and A. Glezer, "Manipulation of a High Aspect Ratio Rectangular Jet," presented at the APS/DFD Meeting, Florida State University, Tallahassee, Florida, November 1992.

[3] Wiltse, J. M. and Glezer, A "Manipulation of free shear flows using piezoelectric actuators," *J. Fluid Mech.*, **249**, 261, 1993.

[4] Jacobs, J.W., James, R. D. Ratliff, C. T. and Glezer A. "Turbulent jets induced by surface actuators," AIAA Paper 93-3243.

[5] Ingard, U. and Labate S. "Acoustic circulation effects and the Nonlinear Impedance of orifices" J. Acoust. Soc. Am. 22, 211-219, 1950.

IV. Plans for next year

- Test prototype pipelined convolution IC when it returns from fabrication.
- Prototype other image processing pipelined processor primitives such as image differencing and resizing.
- Fabricate a practical convolution IC that performs at least 8x8 convolutions on large 8 bit gray scale images. This will build on the information learned from the prototype IC fabricated this year
- Arrays of modulated microjets will be designed, fabricated, and tested.
- A test apparatus containing microjets suitable for mounting and experimental testing in a wind tunnel will be designed and fabricated.

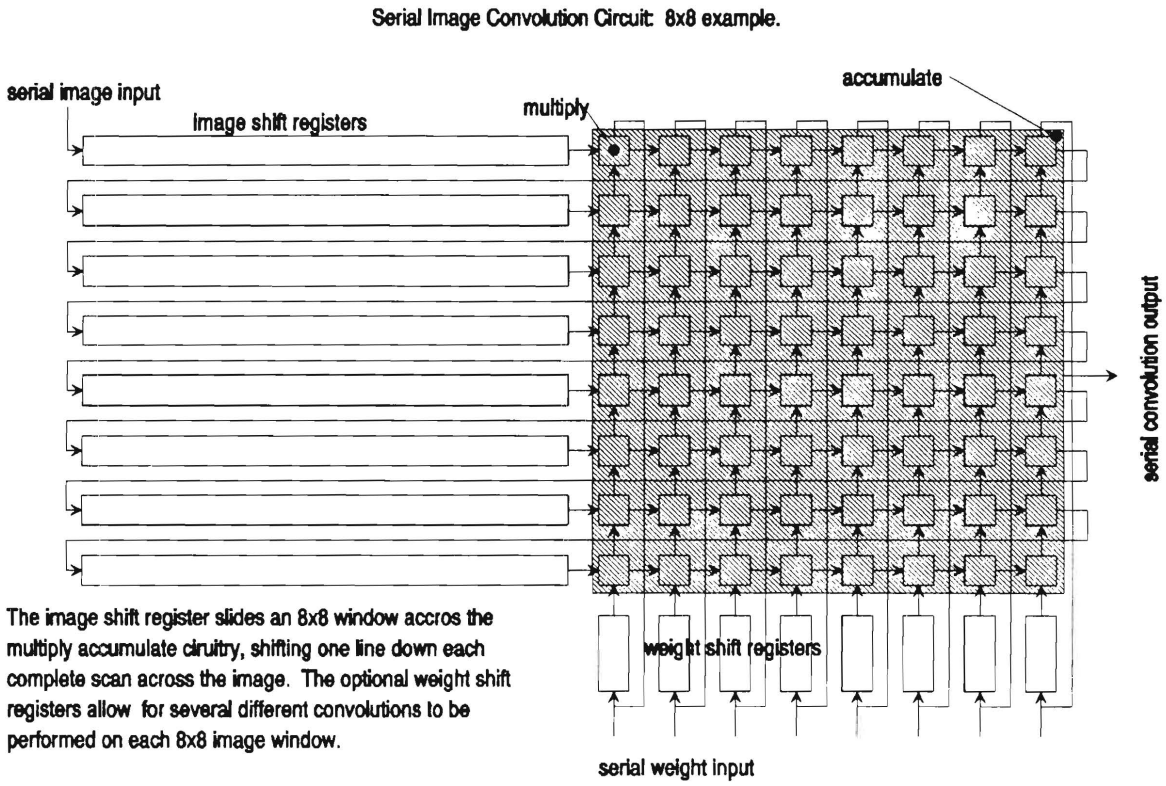

Figure II.1. Pipelined processor for image convolutions.

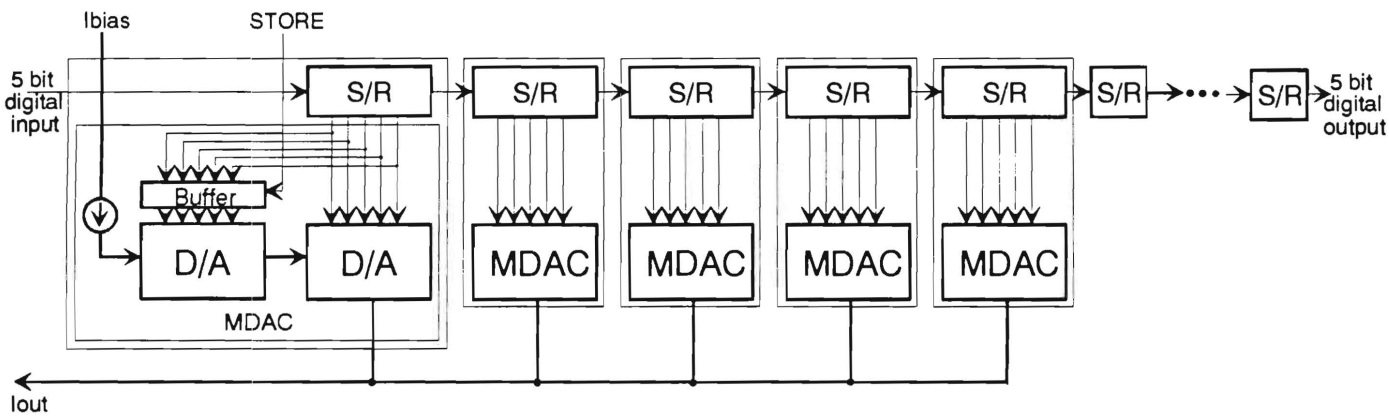

Figure II.2. The block diagram of one row of the processor from Figure 1. The multiplying analog to digital converters (MDACs) perform the multiplies required for the convolution. The accumulate is performed by summing analog currents.

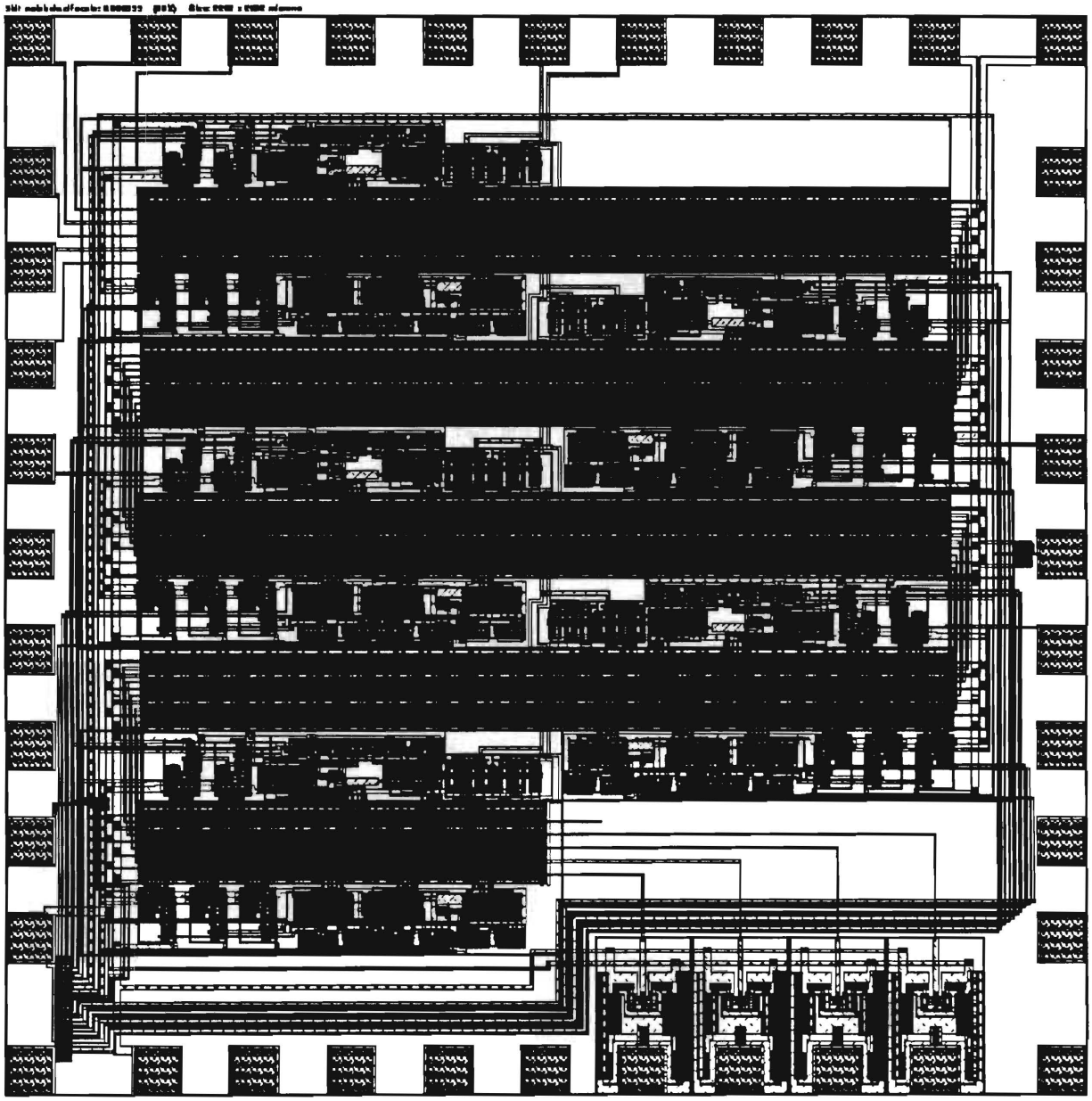

Figure II.3. IC layout for 5 rows of the circuit in Figure 2. The IC is 2.2 x 2.3 millimeters is size. This IC is being fabricated in 2 μm CMOS.

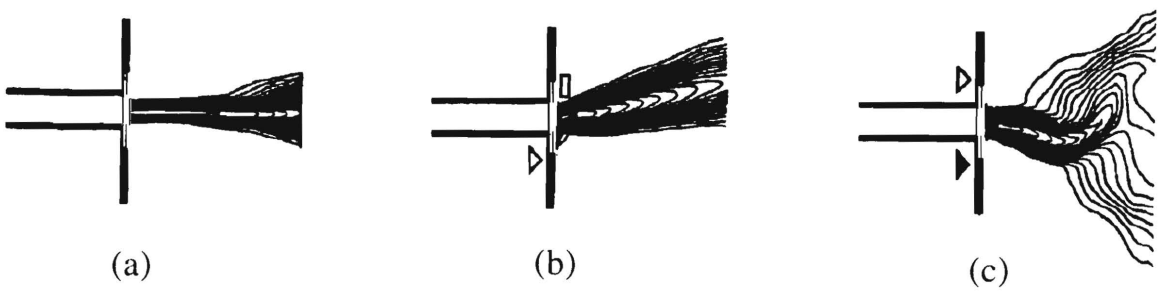

Uexit = 6.5m/s.
Jet width is 1.27cm.
Streamwise domain is 12.7cm

Figure III.1. Measured contours of streamwise velocity for a rectangular air jet with dimensions 7.62 cm x 1.27 cm (exit velocity 6.5 m/s).

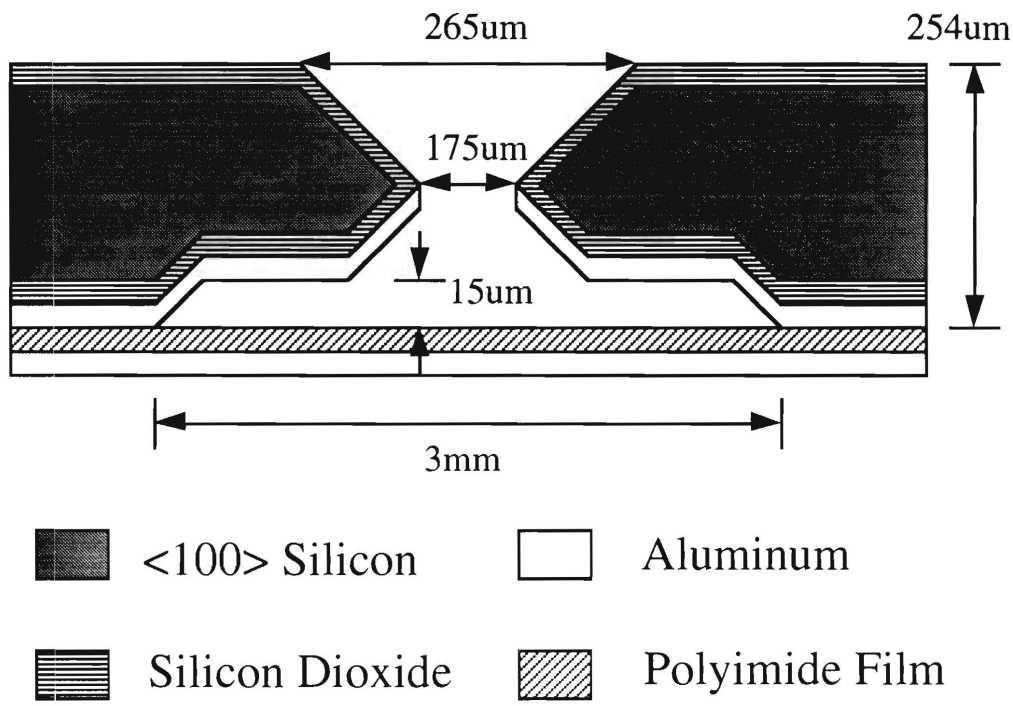

Figure III.2. Cross section of fabricated microjet.

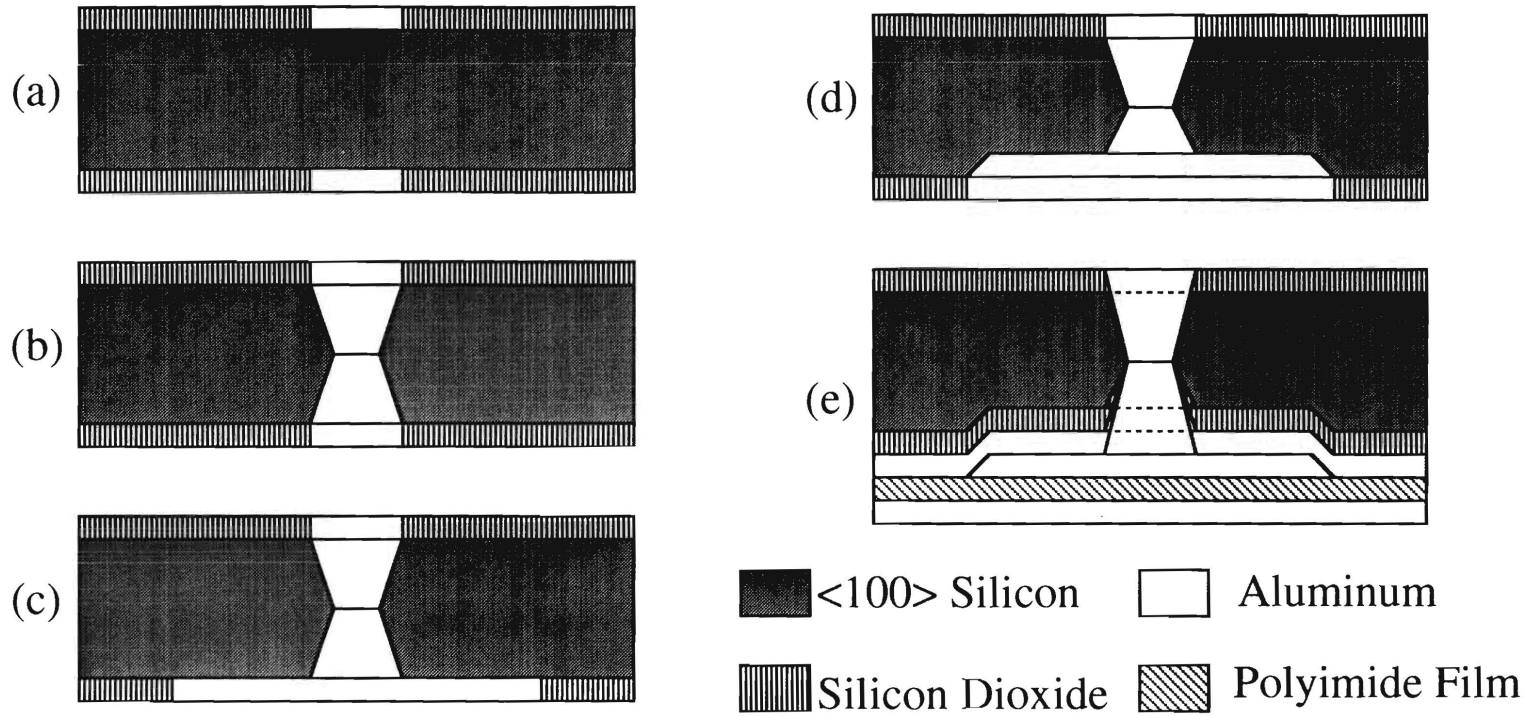

Microjet fabrication sequence.

(a) Prior to etching orifice
(b) After etching orifice
(c) Prior to etching actuator cavity
(d) After etching cavity
(e) After membrane attachment and metallization

Figure III.3. Microjet fabrication sequence. (a) Prior to etching orifice; (b) after etching orifice; (c) prior to etching actuator cavity; (d) after etching cavity; (e) after membrane attachment and metallization.

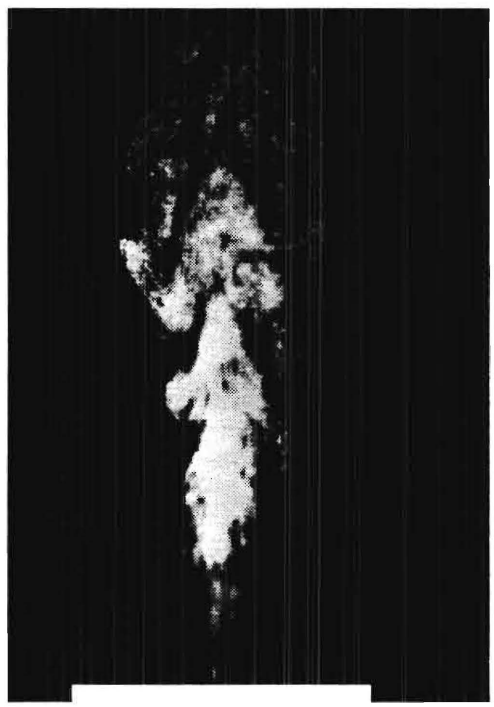

Figure III.4. Smoke visualization of operational microjet.

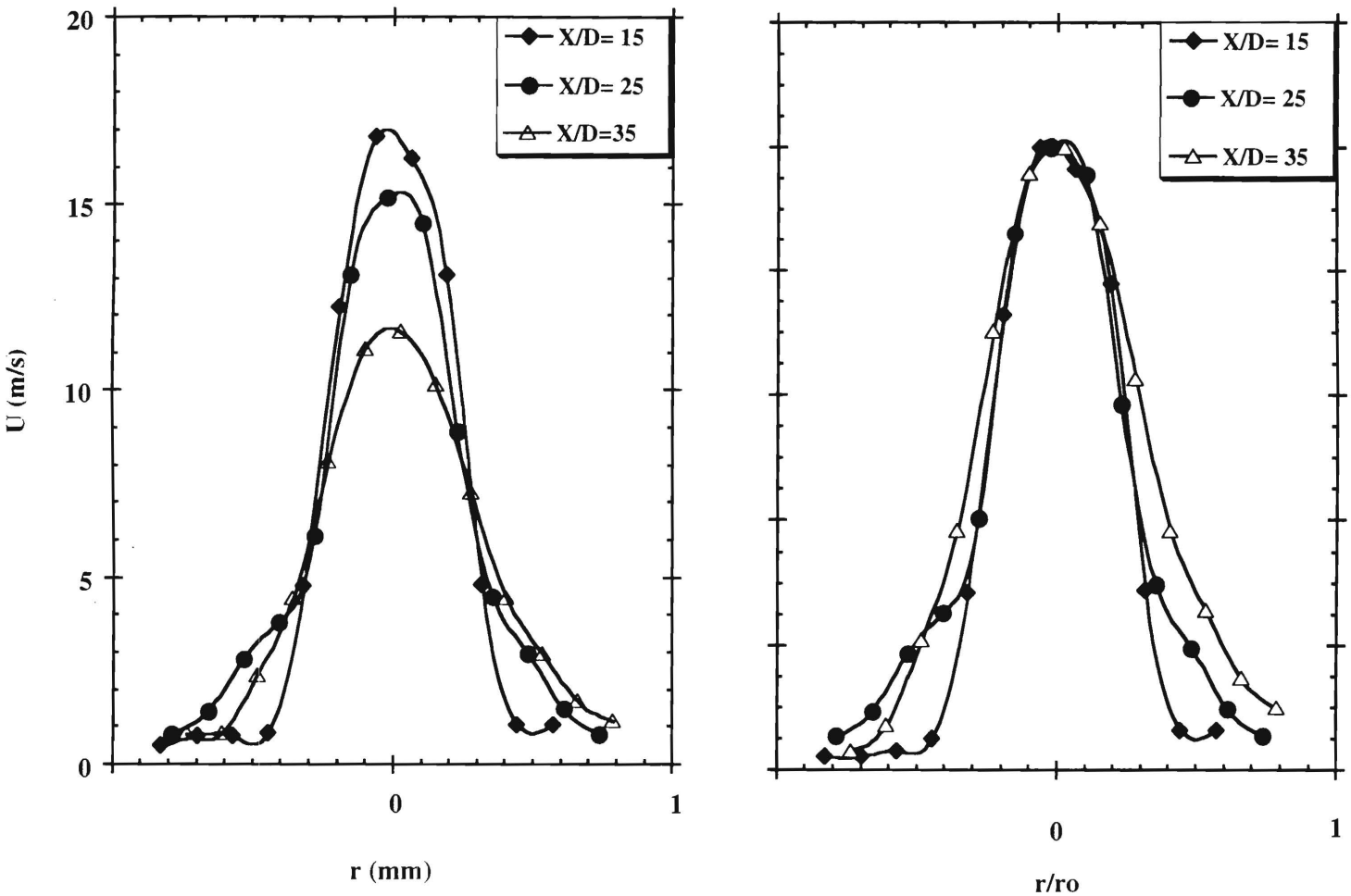

Figure III.5. Measured time-averaged streamwise velocity of the microjet. (a) Plotted using radial coordinates (U in m/s); (b) plotted using similarity variables.

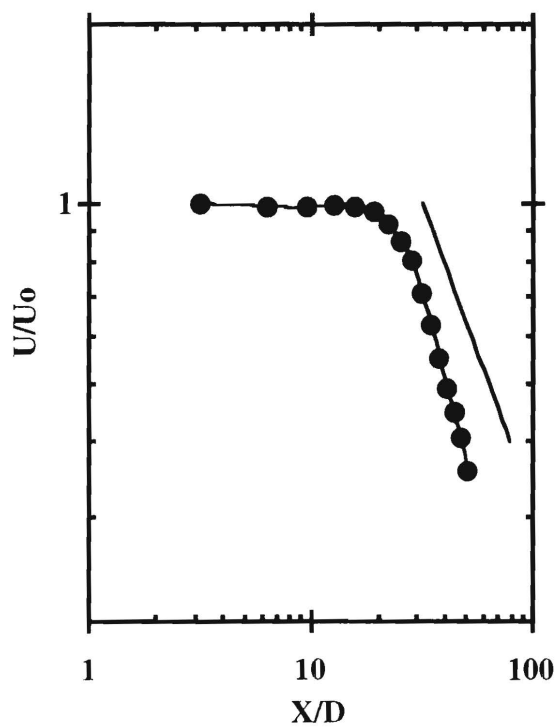

Figure III.6. Measured centerline streamwise velocity decay of microjet.

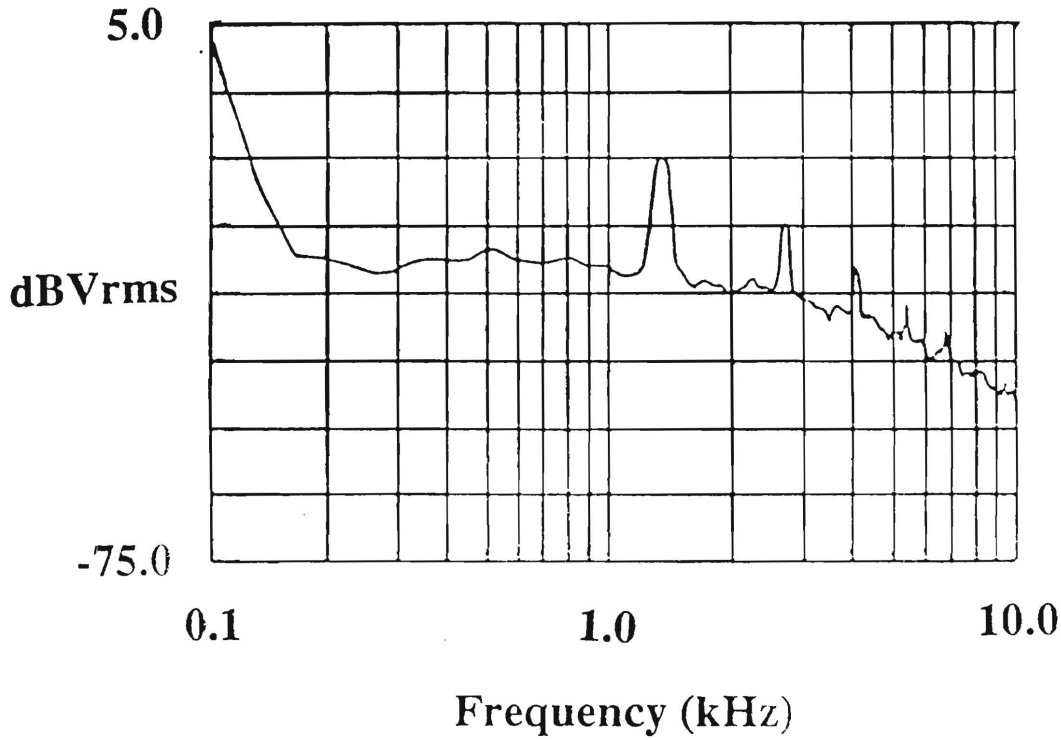

Figure III.7. Frequency spectrum of microjet measured at x/D=40.

E-25-W01
#4

MEMS-BASED DIAGNOSTICS FOR TURBULENT SHEAR FLOWS

AASERT Research Contract F49620-93-1-0495

Progress Report

submitted to:

Dr. James M. McMichael
Air Force Office of Scientific Research

submitted by:

Ari Glezer
Woodruff School of Mechanical Engineering
and
Mark G. Allen and Martin A. Brooke
School of Electrical Engineering
Microelectronics Research Center

Georgia Institute of Technology
Atlanta, GA 30332

Date of Submission: September 1, 1995
Period of Report: September 1, 1994 - September 1, 1995

A. Objectives

The objectives of this work are to develop and exploit micromachined zero mass flux synthetic jet actuators, hereafter referred to as *microjets*. The microjet work is an extension of previous and ongoing work in millimeter scale synthetic jets. The use of micromachining allows the fabrication of small jets, and large arrays of small jets each element of the array being individually controllable. Applications for the microjet technology range from fundamental investigations of flow (including micromixing and the use of microjet arrays to synthesize arbitrarily shaped downstream flow fields for detailed flow studies) to very applied investigations (including direct cooling of electronic components in advanced packaging schemes for high density electronic modules).

B. Abstract of Progress (200 words)

In last year's progress report, the design and fabrication of a micromachined zero-mass-flux synthetic jet, or *microjet*, was presented. In this year's report, the realization of micromachined arrays of these microjets, with each element of the array being individually controllable or modulatable, is presented. The microjet arrays consist of an array small orifices situated on top of an array of actuator cavities bounded by a metallized flexible polyimide diaphragm. The metal electrodes on the diaphragm are patterned so that voltage can be individually applied to the region over each actuator cavity. The membrane is sealed around the cavity and then vibrated using either a piezoelectric transducer or by applying a sinusoidal drive voltage superimposed on the DC bias voltage applied to the flexible diaphragm. Driving the membrane in either fashion results in cavity pressure variations and a jet flow through the orifice. Modulation of an individual jet is achieved by either reducing the amplitude of the drive voltage (for electrostatic drive), or by superimposing a modulation signal onto the bias signal for that element (for piezoelectric drive).

C. Brief Summary of Accomplishments / New Findings

Under this contract, we have previously demonstrated operation of a *single* micromachined synthetic jet actuator (microjet). Arrays of microjets are particularly attractive for applications such as jet vectoring because they can be individually addressed and phased. The use of micromachining fabrication technology for realization of microjet arrays is particularly attractive since the batch fabrication nature of micromachining allows large arrays to be easily fabricated. The research reported here focuses on the fabrication of individually addressable and modulatable microjet arrays and their applications.

The addressable microjet array consists of an array of small orifices situated on top of an array of actuator cavities as in Figure 1. Both the orifices and the cavities are batch

fabricated from (100) silicon using micromachining techniques. The length of an orifice is defined by the wafer thickness, typically 250 μm, while the depth of the actuator cavity is approximately 15 microns. Typical orifice lateral dimensions range from 50-800 μm and typical cavity lateral dimensions range from 1mm to 4mm.

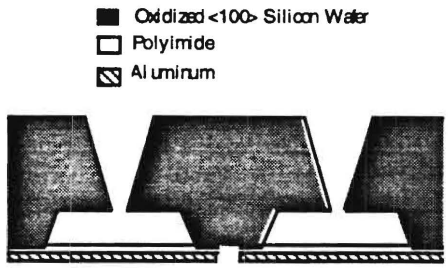

Figure 1. Schematic of microjet array. Two individually controllable orifices are shown.

Individual jet control is achieved by use of a metallized flexible polyimide diaphragm. The metal electrodes on the diaphragm are patterned so that voltage can be individually applied to the region over each actuator cavity. A key feature of this design is that the diaphragm can be vibrated using either a commercial piezoelectric transducer to drive all array elements in parallel, or a sinusoidal drive voltage applied to the flexible diaphragm of individual array elements. Driving the membrane in either fashion results in cavity pressure variations and a jet flow through the orifice. An individual jet is modulated by either reducing the amplitude of the drive voltage of an individual array element (for electrostatic drive) or by electrostatically modulating the diaphragm vibration amplitude for that element (for piezoelectric drive).

Current research has focused on the development of an individually addressable microjet array fabricated with an integrated polyimide membrane. Starting with a high resistivity <100> silicon wafer, a silicon dioxide layer is grown using wet thermal oxidation. The cavity recess is time-etched anisotropically in a potassium hydroxide solution, and the etched recess is filled with electroplated nickel. The orifice is then anisotropically etched in a potassium hydroxide solution from the other side of the wafer using infrared alignment and an oxide etch mask. The integrated polyimide membrane is then formed by spin coating multiple layers of DuPont PI 2611 polyimide onto the front side of the wafer over the nickel-filled cavity recesses. After curing the polyimide, the nickel plugs are removed from the cavity through the orifice hole by wet etching, thus releasing the polyimide membrane for actuation. Finally, the membrane electrode is evaporated onto the top of the membrane through a shadow mask. The silicon wafer itself is used as the second electrode for electrostatic actuation.

In the present work, four electrostatically-modulatable hybrid microjets have been integrated into a 2x2 addressable microjet array driven by a common piezoelectric actuator. Figure 2 shows a Schlieren photograph of an operational 2x2 microjet array taken with a high-speed video camera.

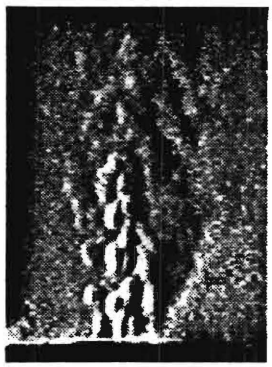

Figure 2. Schlieren photograph of an operational 2x2 microjet array taken with a high-speed video camera

The Schlieren image is obtained by slight heating of the jet cavities. The photograph clearly demonstrates that each of the jets is synthesized by a train of vortex rings. Farther downstream, the jets begin to interact and merge into a single turbulent jet. It is also noted that in the present realization, all jets are driven in phase. Figure 3 shows a time-exposure Schlieren image of two adjacent elements of the addressable array in operation. The flow out of the orifice is visualized by entrainment of helium tracer that is slowly dispensed out of miniature tubes placed near each jet orifice (the tubes are visible in the image). In Figure 3a, both microjets are operating in parallel. Figure 3b shows that the left microjet has been electrostatically-modulated by application of a DC voltage between the array element's membrane electrode and the wafer ground plane electrode. Finally, a larger, 4x5 array of jets has been fabricated. The streamwise velocity distribution along the center row of four jets was measured using a miniature total pressure tube and a 1 mm-Hg pressure transducer (Figure 4). The measurements were taken 4 and 10 mm downstream of the wafer surface using a computer controlled traversing mechanism. At x = 4 mm (open symbols), the four individual jets are clearly distinguishable in the velocity distribution. However, at x = 10 mm (closed symbols), the four jets are virtually merged and the centerline velocity decreases to approximately 4 m/sec.

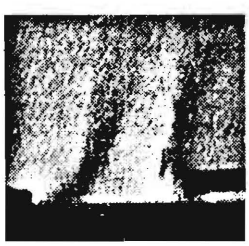

Figure 3a

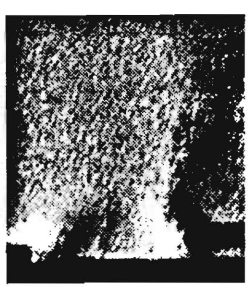

Figure 3b

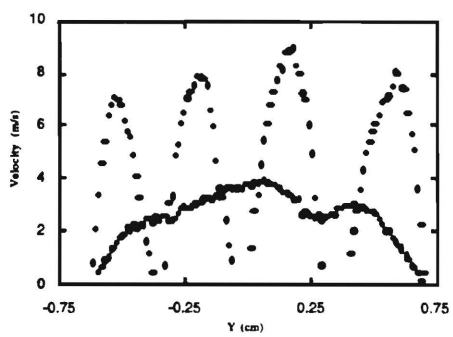

Figure 4

D. List of Personnel

Below is a list of personnel associated with this project and their areas of responsibility:

1. Prof. Mark Allen, School of Electrical and Computer Engineering

Area: Microjet fabrication technology

2. Prof. Martin Brooke, School of Electrical and Computer Engineering

Area: Neural networks for system control

3. Prof. Ari Glezer, School of Mechanical Engineering

Area: Fluid mechanics, microjet physics and behavior

4. Dr. Oliver Brand, School of Electrical and Computer Engineering

Area: Microjet application to electronic cooling

5. Mr. Brent Buchanan, School of Electrical and Computer Engineering

Area: Neural networks for system control

6. Mr. David Coe, School of Electrical and Computer Engineering

Area: Microjet fabrication technology

E. List of Publications

1. D.J. Coe, M. Trautman, M.G. Allen, and A. Glezer, 'Microjets for Manipulation of Macro Flows', Proceedings of the 1994 Solid State Sensor and Actuator Conference, Hilton Head, S.C., June, 1994

2. D.J. Coe, M. Trautman, M.G. Allen, and A. Glezer, 'Addressable Micromachined Jet Arrays', Proceedings of Transducers '95, Eighth International Conference on Solid State Sensors and Actuators, Stockholm, Sweden, June, 1995

F. Interactions / Transitions

Microjet technology is being transitioned in two ways. First, as part of the new Georgia Tech Packaging Research Center, the use of microjets in cooling applications for electronic circuitry is being investigated. Second, the U.S. Army Missile Command has initiated a one year, $120,000 effort to develop microjet cooling technology for missile system electronics. This effort is primarily the responsibility of Dr. Oliver Brand, under the direction of Profs. Allen and Glezer. The deliverable at the end of this project is a simple, 'snap-on' cooler based on microjet technology with internal drivers and circuitry which can be run from standard electronics system voltage levels.

G. New Discoveries, Inventions, Patent Disclosures

A United States Patent application has been filed on aspects of microjet technology in the Summer of 1995.

H. Honors and Awards

None

MEMS-Based Diagnostics

For Turbulent Shear Flows

Annual Progress Report

Grant Number: F49620-93-1-0495

Prepared By:

Prof. Ari Glezer, Mechanical Engineering
Prof. Mark Allen, Electrical and Computer Engineering
Prof. Martin Brooke, Electrical and Computer Engineering

Georgia Institute of Technology
Atlanta, GA 30332

Submitted To:

Dr. James M. McMichael
Air Force Office of Scientific Research
Bolling AFB, DC

Period Covered: September 1, 1995 through August 31, 1996

1. AASERT Student Progress

There are two students being supported on this AASERT grant. Mr. Brent Buchanan is under the direction of Prof. Martin Brooke, and Mr. David Coe is under the direction of Prof. Mark Allen. Both students are making satisfactory progress toward completion of their Ph.D. degrees, as assessed both by their respective advisors as well as the School of Electrical and Computer Engineering. It is anticipated that both students will finish their degrees in 1997.

2. Analog neural net hardware for diagnostic processing

2.1 Objectives

The objective of this section of the research is to develop hardware for fast processing of charge-coupled display (CCD) images. This hardware will take digital CCD output and process it at the same output data rate of the CCD. The result is processed images at the maximum rate possible with a CCD camera. In particular, the hardware will perform convolutions of the input images with a digitally stored convolution kernal matrix, such as are needed for image spatial filtering and neural networks.

2.2 Status of Effort

A hardware test chip has been completed, characterized, and has been used to process images. This chip does not contain the digital front end necessary to connect directly to a CCD data stream but does demonstrate all of the critical analog components of the image processor. The test chip will be integrated with a shift register in a later chip fabrication to produce a fully functional image processor chip capable of connection to the data stream directly output from a CCD or similar row-wise serial output imaging device.

2.3 Accomplishments

2.3.1 Spatially Oversampled Filtering Theory

Since physical impracticalities prevent the straight-forward and compact design of high-order bit A/D converters in standard digital fabrication processes, it is desirable to develop an architectural design philosophy that can incorporate the low level of component precision that is readily available while concurrently achieving a suitably high system performance. A successful methodology that is now commonly used with the sampling of audio signals, Delta-Sigma Quantization, involves signal oversampling and quantization noise shaping to produce a signal represented by small bit lengths, though at the expense of greater temporal granularization. This technique is readily extended to multi-dimensional signals such as images.

Intuitively, this procedure works by increasing the operational spectrum beyond the Nyquist demands of the signal and forcing the quantization noise energy into the unused portions of the widened spectrum. As the noise energy in the signal band is displaced, the in-band signal-to-noise ratio (SNR) increases though the total SNR remains the same (or, as in actual practice, slightly deteriorates) for a given level of quantization. This permits the

signal to be represented with shorter bit-length samples, though more of them, and without compromising the information content of the signal. As long as the noise energy is not aliased into the signal band during subsequent processing steps, it may be harmlessly transported through the overall system or filtered off if necessary.

2.3.2 Image Processing Hardware Test Chip

A hardware test chip has been completed. The chip contains the analog-digital mixed signal portion of the proposed CCD image processing circuit. Specifically, this chip contains 512 A/D converters arranged in a 16x16 array of Multiplying A/D Converters (MDACs). Each of the 256 MDACs consists of two 5-bit A/D converters, two 5-bit digital storage registers, and a sign register. After the appropriate weight from the convolution kernel and pixel data from the image have been stored in the two storage registers, the multiplication is performed through the biasing of the data A/D Converter with the output of the weight A/D Converter. The sign register stores a bit which determines to which of two universally common nodes the output current is then tied. With one node corresponding to positive weights and the other negative weights, the difference in the output of these currents from the entire array of MDACs is then the result of the current convolution point.

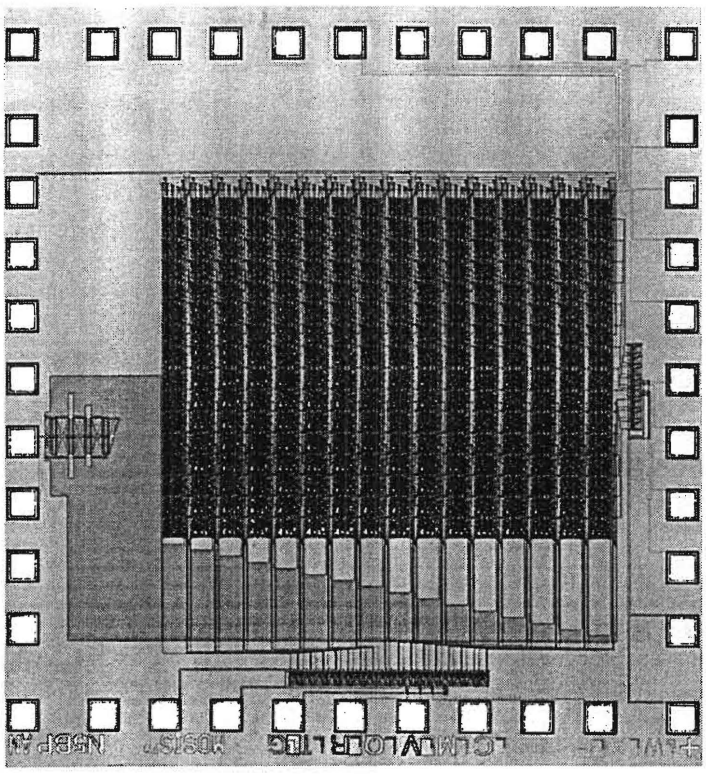

Figure 1: Analog Convolution Chip

This chip has been tested for its ability to perform image processing tasks such as spatial filtering.

After characterizing the entire array of MDACs for performance and matching, a low-pass characteristic convolution kernel (a 16x16 "Mexican hat") was programmed into the weight registers and an image (Figure 2a) was passed through the chip with the use of an automated test bed. The test bed consisted of a PC with a digital output card running under LabView, and two SMUs under observation by a GPIB controller installed in the same PC. For purposes of comparison, an `ideal' resultant image was computed with a compiled using a compiled C program specially written for the purpose (Figure 2b). The image observed by the automated test bed appears in Figure 2c. Note that the circuit successfully removed the high frequency components of the original image while passing the low frequency portions of the image, but introduced a degree of high frequency (presumably broad spectrum) noise likely due to quantization effects.

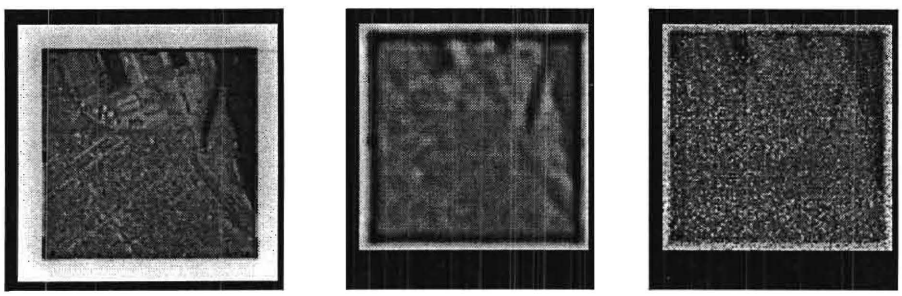

(a) (b) (c)

Figure 2. Chip input and output images. (a) 128x128 input image; (b) 113x113 computer generated floating-point output image; (c) 113x113 chip-generated mixed-signal output image

3. Microjet Hardware for Flow Manipulation

3.1 Objectives

The objective of this phase of the effort is to develop microjet-based actuators which have the capability of affecting and manipulating flows. Ultimately it is hoped that these actuators can be coupled with appropriate (e.g., analog-hardware-based) sensing and control schemes such as those described above to create a complete flow manipulation system.

3.2 Status of Effort

New drive elements based on electromagnetic drive have been investigated to reduce unwanted noise emitted by the jet generation actuators. In addition, a scheme to produce more robust microjets with an eye towards eventually being able to manipulate flows of practical aerodynamic interest has been investigated and is currently under development. This scheme involves the use of conventional drivers to generate higher-momentum microjet arrays, and highly interconnected and batch fabricated modulators at the output of each orifice hole of the array to control and modulate the robust jet output. Successful modulation of jets in excess of 20 m/s using batch-fabricated, MEMS-based modulators has been achieved.

In the robust designs, the microjet array consists of a silicon wafer with an array of anisotropically-etched orifices through the wafer. A bimetallic beam is suspended above each orifice to serve as the valve flap. Attached to the back of the wafer is an external membrane driven continuously by either a piezoelectric or electromagnetic driving element. When an electrical current is passed through a particular bimetallic beam structure, the resulting heat causes the beam structure to bend (either vertically or horizontally, depending upon the design) uncovering an orifice to allow a synthetic jet to flow through it. The advantage of this microjet design is that it decouples the jet generation and jet modulation functions, thereby reducing the demands on the microactuator elements and simplifying fabrication.

3.3 Accomplishments

3.3.1 Drive Element

Previous microjet devices have been driven with an external piezoelectric element operating at 1.3 kHz. The disadvantages of such devices included relatively high operating voltages (up to 42Vrms) and the unpleasant audible noise due to operation. A new electromagnetic driving element is now being used for microjet research. This new drive element produces jets comparable to those generated by the piezoelectric element yet it operates at lower voltages (8-10V_{pp}) with low power dissipation (up to 300mW). Moreover, the electromagnetic driver operates at a lower frequency range, 150-200Hz, generating considerably less audible noise than previously reported microjet devices.

3.3.2 Modulator Fabrication

Both electrostatic and bimetallic (thermal) actuators as modulators are under consideration. The fabrication sequence for the bimetallic modulators is as follows. Starting with an oxidized <100> silicon substrate, standard photolithography is used to transfer the orifice pattern into the oxide layer on the front side of the wafer. In the second photolithography step, infrared alignment is used to align the same pattern to the oxide layer on the back side of the layer. A sacrificial layer material, such as photoresist or aluminum, is then deposited on the front side of the wafer and patterned using conventional photolithography. An electroplating seed layer is sputtered over the front surface of the wafer. Copper is electroplated into a patterned plating mold to the desired thickness. Nickel/iron is then electroplated on top of the copper using the same mold. The structure release sequence begins with removal of the electroplating mold and exposed seed layer. The sacrificial material is then etched to release the structure prior to submerging the wafer into a heated potassium hydroxide solution that etches the orifice holes through the wafer.

Significant progress towards fabrication of a complete valve-based microjet device has been made. Theoretical flap deflection models have been constructed for flaps of various dimensions and material compositions. Shown in Figure 3 are photographs of fabricated devices. Figure 3a shows a variety of bimetallic structures fabricated on a glass substrate for deflection testing. Figure 3b shows a photograph of a fabricated 2x2 microjet array prior to driver attachment. The orifices are located in the top center of the photograph under the tips of the cantilever beam modulators.

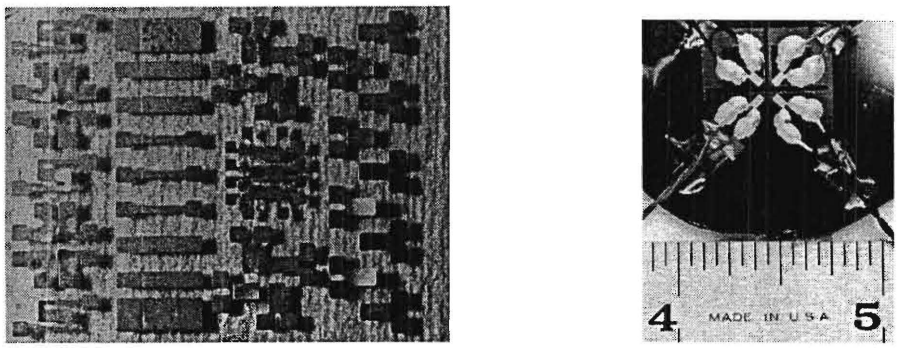

(a) (b)

Figure 3. Fabricated modulators and microjets. (a) Photograph of fabricated bimetallic flap test structures on glass substrate; (b) Photograph of fabricated 2x2 valve-based microjet array prior to attachment of external membrane and driver. An orifice is located under the tip of each micromachined beam. Test leads are also visible in this photograph. Ruler scale is in inches.

4. Publications

1. Wills, D. S., Lacy, W. S., Camperi-Ginestet, C., Buchanan, B., Jokerst, N. M., Brooke, M. A., "A Fine-Grain, High-Throughput Architecture Using Through-Wafer Optical Communication," *IEEE Journal of Lightwave Technology*, Vol. 13, No. 4, pp. 1085-1092, June, 1995.

2. N. M. Jokerst, C. Camperi-Ginestet, B. Buchanan, S. Wilkinson, M. Brooke, "Communication Through Stacked Silicon Circuitry Using Integrated Thin Film InP-Based Emitters and Detectors," *IEEE Photonics Technology Letters*, Vol. 7, No. 9, pp. 1028-1030, September, 1995.

3. N. Jokerst, M. Brooke, O. Vendier, S. Wilkinson, S. Fike, M. Lee, E. Twyford, J. Cross, B. Buchanan, S. Wills, "Thin Film Multimaterial Optoelectronic Integrated Circuits," *IEEE Transactions on Components, Packaging, and Manufacturing Technology, Part B*, Vol. 19, No. 1, February, 1996, Invited.

MEMS-Based Diagnostics

For Turbulent Shear Flows

Final Technical Report

Grant Number: F49620-93-1-0495

Prepared By:

Prof. Ari Glezer, Mechanical Engineering
Prof. Mark Allen, Electrical and Computer Engineering
Prof. Martin Brooke, Electrical and Computer Engineering

Georgia Institute of Technology
Atlanta, GA 30332

Submitted To:

Drs. James M. McMichael / Mark Glauser
Air Force Office of Scientific Research
Bolling AFB, DC

1. AASERT Student Progress

There are two students who have been supported on this AASERT grant. Mr. Brent Buchanan is under the direction of Prof. Martin Brooke, and Mr. David Coe is under the direction of Prof. Mark Allen. Both students are making satisfactory progress toward completion of their Ph.D. degrees, as assessed both by their respective advisors as well as the School of Electrical and Computer Engineering. It is anticipated that both students will finish their degrees in 1997 (this year).

Mr. Buchanan has primarily been responsible for development of neural network architectures for deconvoluting flow information from flow sensors which have either been embedded into the flow or which have used optical means to sense flow information. Mr. Coe has been responsible for the development of a new class of actuators, the micromachined jet or *microjet*, which is a micromachined synthetic jet capable of momentum injection (but no mass injection) into the flow.

Only summaries of the work are given in the report. Full details are given in the previous progress reports as well as scientific papers in the references, most of which have been previously submitted to AFOSR.

2. Analog neural net hardware for diagnostic processing

2.1 Objectives

The objective of this section of the research is to develop hardware for fast processing of charge-coupled display (CCD) images. This hardware will take digital CCD output and process it at the same output data rate of the CCD. The result is processed images at the maximum rate possible with a CCD camera. In particular, the hardware will perform convolutions of the input images with a digitally stored convolution kernal matrix, such as are needed for image spatial filtering and neural networks.

2.2 Status of Effort

A hardware test chip has been completed, characterized, and has been used to process images. This chip does not contain the digital front end necessary to connect directly to a CCD data stream but does demonstrate all of the critical analog components of the image processor. The test chip will be integrated with a shift register in a later chip fabrication to produce a fully functional image processor chip capable of connection to the data stream directly output from a CCD or similar row-wise serial output imaging device.

2.3 Accomplishments

2.3.1 Spatially Oversampled Filtering Theory

Since physical impracticalities prevent the straight-forward and compact design of high-order bit A/D converters in standard digital fabrication processes, it is desirable to develop an architectural design philosophy that can incorporate the low level of component precision that is readily available while concurrently achieving a suitably high system performance. A successful methodology that is now commonly used with the sampling of

audio signals, Delta-Sigma Quantization, involves signal oversampling and quantization noise shaping to produce a signal represented by small bit lengths, though at the expense of greater temporal granularization. This technique is readily extended to multi-dimensional signals such as images.

Intuitively, this procedure works by increasing the operational spectrum beyond the Nyquist demands of the signal and forcing the quantization noise energy into the unused portions of the widened spectrum. As the noise energy in the signal band is displaced, the in-band signal-to-noise ratio (SNR) increases though the total SNR remains the same (or, as in actual practice, slightly deteriorates) for a given level of quantization. This permits the signal to be represented with shorter bit-length samples, though more of them, and without compromising the information content of the signal. As long as the noise energy is not aliased into the signal band during subsequent processing steps, it may be harmlessly transported through the overall system or filtered off if necessary.

2.3.2 Image Processing Hardware Test Chip

A hardware test chip has been completed. The chip contains the analog-digital mixed signal portion of the proposed CCD image processing circuit. Specifically, this chip contains 512 A/D converters arranged in a 16x16 array of Multiplying A/D Converters (MDACs). Each of the 256 MDACs consists of two 5-bit A/D converters, two 5-bit digital storage registers, and a sign register. After the appropriate weight from the convolution kernel and pixel data from the image have been stored in the two storage registers, the multiplication is performed through the biasing of the data A/D Converter with the output of the weight A/D Converter. The sign register stores a bit which determines to which of two universally common nodes the output current is then tied. With one node corresponding to positive weights and the other negative weights, the difference in the output of these currents from the entire array of MDACs is then the result of the current convolution point. This chip has been tested for its ability to perform image processing tasks such as spatial filtering.

After characterizing the entire array of MDACs for performance and matching, a low-pass characteristic convolution kernel (a 16x16 "Mexican hat") was programmed into the weight registers and an image (Figure 2a) was passed through the chip with the use of an automated test bed. The test bed consisted of a PC with a digital output card running under LabView, and two SMUs under observation by a GPIB controller installed in the same PC. For purposes of comparison, an `ideal' resultant image was computed with a compiled using a compiled C program specially written for the purpose (Figure 2b). The image observed by the automated test bed appears in Figure 2c. Note that the circuit successfully removed the high frequency components of the original image while passing the low frequency portions of the image, but introduced a degree of high frequency (presumably broad spectrum) noise likely due to quantization effects.

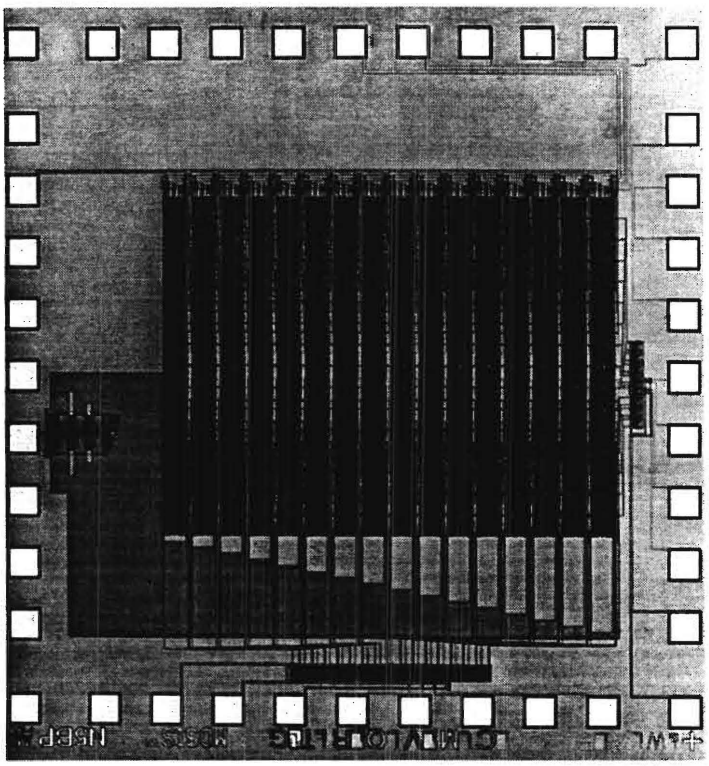

Figure 1: *Analog Convolution Chip*

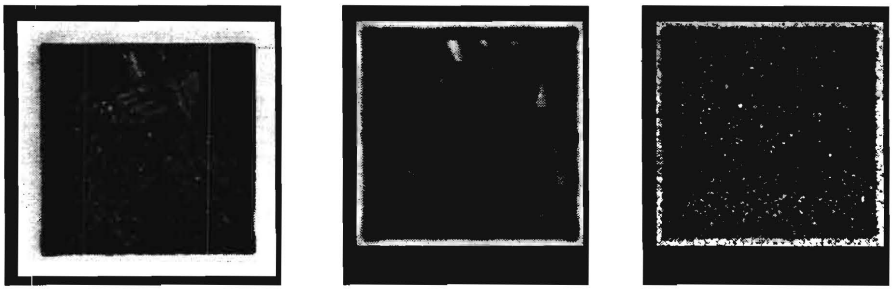

(a) (b) (c)

Figure 2. *Chip input and output images. (a) 128x128 input image; (b) 113x113 computer generated floating-point output image; (c) 113x113 chip-generated mixed-signal output image*

3. Microjet Hardware for Flow Manipulation

3.1 Objectives

The objective of this phase of the effort is to develop microjet-based actuators which have the capability of affecting and manipulating flows. Ultimately it is hoped that these actuators can be coupled with appropriate (e.g., analog-hardware-based) sensing and control schemes such as those described above to create a complete flow manipulation system.

3.2 Status of Effort

Under this AASERT contract, synthetic jet technology which was developed under the parent grant has been implemented using standard (traditional) MEMS technology. A cross-section of a prototype micromachined version of the synthetic jet which has been developed at Georgia Tech [4,6] is shown in Figure 3. The polyimide film acts as a flexible diaphragm, the vibration of which causes jet emission from the orifice hole. Both integrated electrostatic excitation of the diaphragm (by applying a sinusoidal voltage between the two aluminum electrodes) as well as external drive of the diaphragm (e.g., by using a piezoelectric driving element) have been successfully used to realize microjets. A smoke visualization of the micromachined jet (rotated 90 degrees) is shown in Figure 4. The field of view measures 89 mm in the streamwise (x) direction and thus corresponds to nearly 500 jet diameters. The jet appears to become turbulent at or near the orifice, and spreads almost linearly with streamwise distance. Large coherent vortical structures are apparent in the far field of the jet. The Reynolds number of the jet based on the centerline velocity and its width at x/D = 15 (see velocity profiles in Figure 5) is approximately 1400.

The streamwise velocity component was measured using a miniature total pressure tube having inner and outer diameters of 212 μm and 340 μm, respectively. Radial profiles of the time-averaged streamwise velocity were measured at x/D = 15, 25, and 35 using a three-axis traversing mechanism. peak jet velocities of 15-20 m/s were achieved 15 diameters downstream of the orifice hole. The jet is reasonably symmetric about its centerline, and when jet velocity profiles are plotted in similarity coordinates they collapse reasonably well on top of each other, suggesting that the jet is self-similar.

This work has also been extended to micromachined jet arrays which are individually addressable [4]. The addressable microjet array consists of an array of small orifices situated on top of an array of actuator cavities. Both the orifices and the cavities are batch fabricated from (100) silicon using micromachining techniques. The length of an orifice is defined by the wafer thickness, typically 250 μm, while the depth of the actuator cavity is approximately 15 microns. Typical orifice lateral dimensions range from 50-800 μm. Individual jet control is achieved by use of a metallized flexible polyimide diaphragm, or by use of electrothermally driven modulators at each orifice. The metal electrodes on the diaphragm are patterned so that voltage can be individually applied to the region over each actuator cavity. Similarly to the individual microjets, the diaphragm can be vibrated using either a commercial piezoelectric transducer to drive all array elements in parallel or a sinusoidal drive voltage applied to the flexible diaphragm of individual array elements. Driving the membrane in either fashion results in cavity pressure variations and a jet flow through the orifice. An individual jet is modulated by either reducing the amplitude of the drive voltage of an individual array element (for electrostatic drive) or by electrostatically modulating the diaphragm vibration amplitude for that element (for piezoelectric drive).

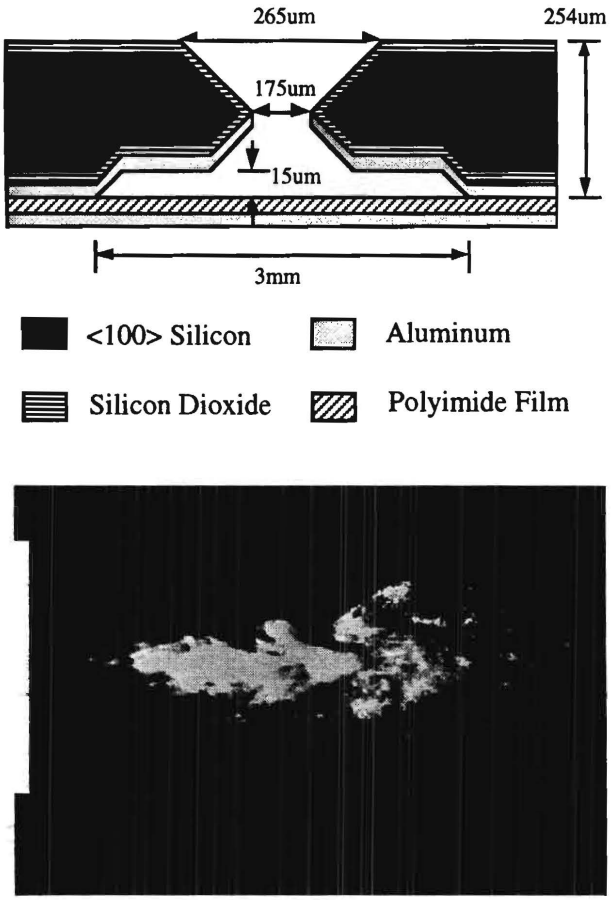

Figure 3. *Left: Schematic of micromachined synthetic jet; Right: Smoke visualization of operational jet.*

The above hardware demonstrates that it is feasible to use MEMS technology to microfabricate arrays of individually addressable synthetic jets. Recently, new drive elements based on electromagnetic drive have been investigated to reduce unwanted noise emitted by the jet generation actuators. In addition, a scheme to produce more robust microjets with an eye towards eventually being able to manipulate flows of practical aerodynamic interest has been investigated and is currently under development. This scheme involves the use of conventional drivers to generate higher-momentum microjet arrays, and highly interconnected and batch fabricated modulators at the output of each orifice hole of the array to control and modulate the robust jet output. Successful modulation of jets in excess of 20 m/s using batch-fabricated, MEMS-based modulators has been achieved.

In the robust designs, the microjet array consists of a silicon wafer with an array of anisotropically-etched orifices through the wafer. A bimetallic beam is suspended above each orifice to serve as the valve flap. Attached to the back of the wafer is an external membrane driven continuously by either a piezoelectric or electromagnetic driving element. When an electrical current is passed through a particular bimetallic beam structure, the resulting heat causes the beam structure to bend (either vertically or horizontally, depending upon the design) uncovering an orifice to allow a synthetic jet to flow through it. The advantage of this microjet design is that it decouples the jet generation and jet modulation functions, thereby reducing the demands on the microactuator elements and simplifying fabrication.

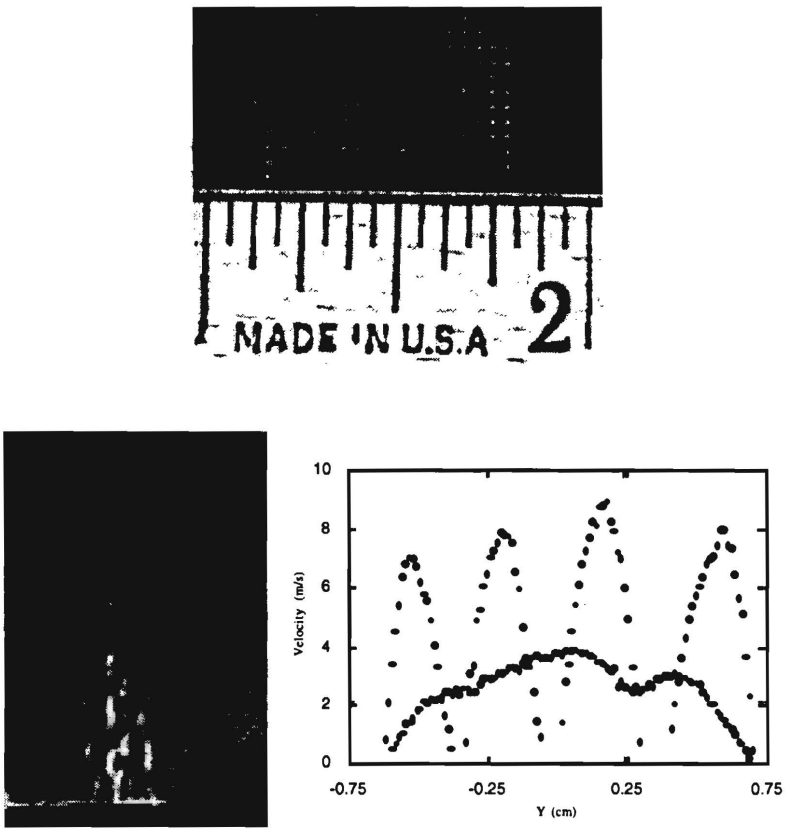

Figure 4. *Top: Photomicrograph of microjet array; bottom left: Schlieren visualization of an operating 4x4 array; bottom right: velocity profiles of near-field emerging jets (4 distinct peaks) and far field merged jet.*

3.3 Accomplishments

3.3.1 Drive Element

Previous microjet devices have been driven with an external piezoelectric element operating at 1.3 kHz. The disadvantages of such devices included relatively high operating voltages (up to 42Vrms) and the unpleasant audible noise due to operation. A new electromagnetic driving element is now being used for microjet research. This new drive element produces jets comparable to those generated by the piezoelectric element yet it operates at lower voltages (8-10V_{pp}) with low power dissipation (up to 300mW). Moreover, the electromagnetic driver operates at a lower frequency range, 150-200Hz, generating considerably less audible noise than previously reported microjet devices.

3.3.2 Modulator Fabrication

Both electrostatic and bimetallic (thermal) actuators as modulators are under consideration. The fabrication sequence for the bimetallic modulators is as follows. Starting with an oxidized <100> silicon substrate, standard photolithography is used to transfer the orifice pattern into the oxide layer on the front side of the wafer. In the second photolithography step, infrared alignment is used to align the same pattern to the oxide layer on the back side of the layer. A sacrificial layer material, such as photoresist or aluminum, is then deposited on the front side of the wafer and patterned using conventional

photolithography. An electroplating seed layer is sputtered over the front surface of the wafer. Copper is electroplated into a patterned plating mold to the desired thickness. Nickel/iron is then electroplated on top of the copper using the same mold. The structure release sequence begins with removal of the electroplating mold and exposed seed layer. The sacrificial material is then etched to release the structure prior to submerging the wafer into a heated potassium hydroxide solution that etches the orifice holes through the wafer.

Significant progress towards fabrication of a complete valve-based microjet device has been made. Theoretical flap deflection models have been constructed for flaps of various dimensions and material compositions. Shown in Figure 3 are photographs of fabricated devices. Figure 3a shows a variety of bimetallic structures fabricated on a glass substrate for deflection testing. Figure 3b shows a photograph of a fabricated 2x2 microjet array prior to driver attachment. The orifices are located in the top center of the photograph under the tips of the cantilever beam modulators.

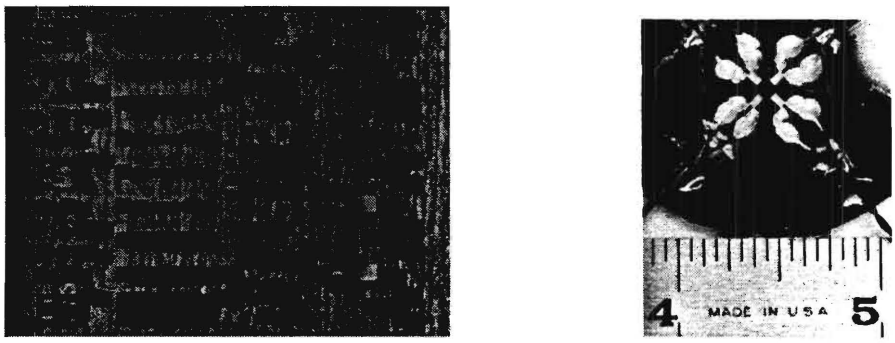

(a) (b)

Figure 5. *Fabricated modulators and microjets. (a) Photograph of fabricated bimetallic flap test structures on glass substrate; (b) Photograph of fabricated 2x2 valve-based microjet array prior to attachment of external membrane and driver. An orifice is located under the tip of each micromachined beam. Test leads are also visible in this photograph. Ruler scale is in inches.*

In addition to the silicon-based microjet actuators, the concept of robust devices initiated in this grant has been expanded and leveraged using other contracts to expand the materials base. An example of this is given for electronic cooling applications below.

An example of this approach to fabricate large-area microjets intended for electronic cooling applications is given below. The actuator consists of a corrugated parylene membrane carrying a stencil-printed permanent magnet, and is approximately 1 cm in diameter. A planar coil for electromagnetic actuation is fabricated on the other side of the substrate. A commercially available printed circuit board with a single copper layer is used as substrate material. In a first step, 1 cm recess holes defining the final membrane sizes are drilled into the laminated epoxy board from the backside (Figure 6 (top left)). Additional 1 mm holes are drilled through the substrate in the membrane center to allow the final sacrificial layer etch. A copper foil is laminated onto the backside of the epoxy substrate in a press with a force and temperature of 3.125 tons and 100 °C, respectively. The lamination process forms circular copper membranes with a diameter of 1 cm suspended over the recess holes. A corrugation profile and a flat zone in the membrane center are then etched into the copper layer. The 14 circular corrugations have a height of 80 μm and a period of 200 μm. Then, a 2 μm parylene film is deposited by plasma coating on top of the corrugated copper membranes. Polymer permanent magnets [5] with a diameter of 4 mm, and a thickness of 1 mm are stencil-printed onto the flat zone in the

membrane center. After curing and remagnetizing the magnet, the copper in the area of the diaphragms is etched through the 1 mm holes in a ferric chloride solution. A photograph of the corrugated parylene membrane with the stencil-printed polymer magnet is shown in Figure 6 (bottom). Once the parylene diaphragms are released, the planar coils are fabricated on the opposite side of the substrate using standard photolithography (Figure 6 (top right)). The planar, square coil consists of 31 turns with a wire thickness of 15 μm, and a width and spacing of 40 μm. The planar coils have a typical resistance of 20 to 30 Ω. Instead of a stencil-printed polymer magnet, a commercially available Nd-Fe-B magnet can be mounted in an hybrid fashion onto the parylene diaphragms. Both types of magnetic microactuators have been fabricated.

The fabricated actuators have maximum deflections of 60 μm at 100 mA for NdFeB magnets, and 35 μm at 300 mA for the polymer magnet have been achieved. Under AC excitation, the actuators are audible in the range from 1 to 3 kHz, and produce the strongest synthetic jets in the 50-100 Hz range. It is anticipated that even though the AASERT funding is now ended, this development of robust microjet actuators will continue.

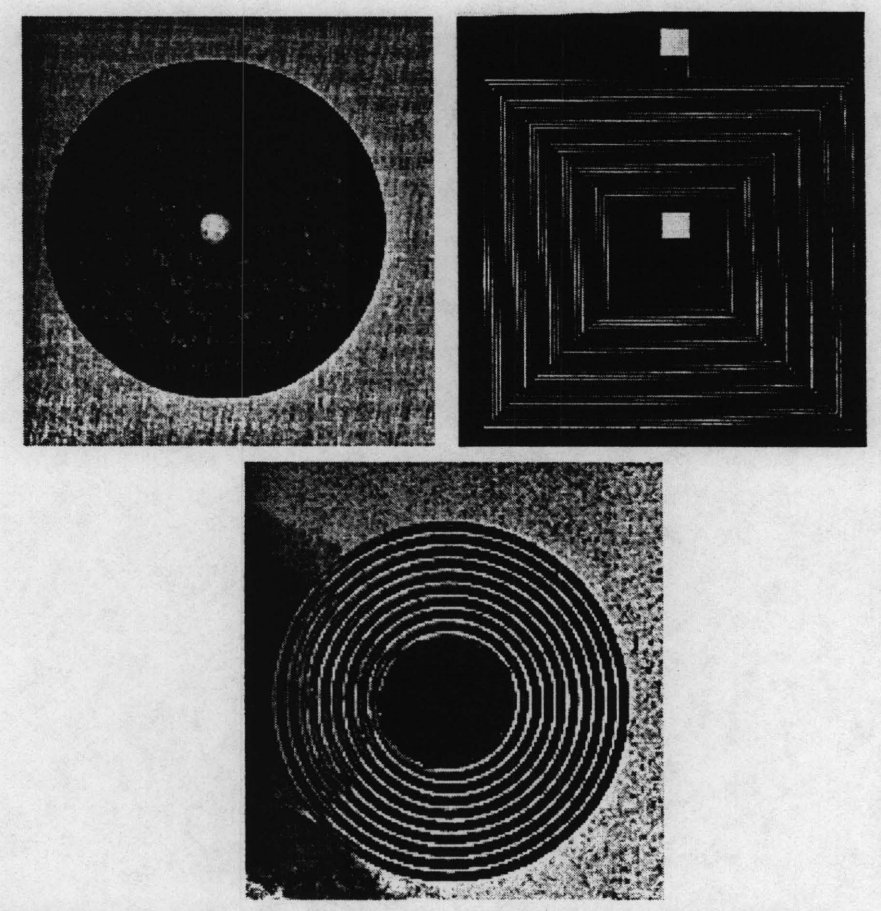

***Figure 6** Large area microjet during various stages of fabrication*

4. Publications

1. Wills, D. S., Lacy, W. S., Camperi-Ginestet, C., Buchanan, B., Jokerst, N. M., Brooke, M. A., "A Fine-Grain, High-Throughput Architecture Using Through-Wafer Optical Communication," *IEEE Journal of Lightwave Technology*, Vol. 13, No. 4, pp. 1085-1092, June, 1995.

2. N. M. Jokerst, C. Camperi-Ginestet, B. Buchanan, S. Wilkinson, M. Brooke, "Communication Through Stacked Silicon Circuitry Using Integrated Thin Film InP-Based Emitters and Detectors," *IEEE Photonics Technology Letters*, Vol. 7, No. 9, pp. 1028-1030, September, 1995.

3. N. Jokerst, M. Brooke, O. Vendier, S. Wilkinson, S. Fike, M. Lee, E. Twyford, J. Cross, B. Buchanan, S. Wills, "Thin Film Multimaterial Optoelectronic Integrated Circuits," *IEEE Transactions on Components, Packaging, and Manufacturing Technology, Part B*, Vol. 19, No. 1, February, 1996, Invited.

4. Coe, D.J.; Allen, M.G.; Smith, B.L.; Glezer, A. "Addressable micromachined jet arrays", 8th International Conference on Solid-State Sensors and Actuators and Eurosensors IX . Digest of Technical Papers, p.329-32 vol.2, 1995

5. Lagorce, L., and Allen, M.G., "Micromachined Polymer Magnets", 1996 IEEE Microelectromechanical Systems Meeting, Technical Digest, San Diego, CA, February, 1996

6. Coe, D.J.; Allen, M.G.; Smith, B.L.; Glezer, A. "Micromachined Jets for Manipulation of Macro Flows", 1994 Solid State Sensors and Actuators Conference, Hilton Head, SC, 1994